Zebrafish irradiation

The effects of high dose-rate radiation on zebrafish embryos

by

B.L. Crum

to obtain the degree of Master of Science
at the Delft University of Technology,
to be defended publicly on Wednesday January 29, 2020 at 10:30 AM.

Student number:	4705378	
Project duration:	March 1, 2019 – January 29, 2020	
Thesis committee:	Dr. ir. D.R. Schaart	TU Delft, chair
	Dr. E. C. M. Carroll,	TU Delft, supervisor
	Dr. Z. Perkó,	TU Delft, supervisor
	Dr. ir. A. G. Denkova,	TU Delft, member

This thesis is confidential and cannot be made public until December 31, 2021.

TU Delft

Abstract

Finding a favorable cure for cancer has been one of the main clinical challenges today. Nowadays the majority of the patients is treated with radiotherapy. Recently research in to a new paradigm of radiotherapy, so called FLASH radiotherapy, has opened up a new insight in to reducing negative side effects. FLASH dose rates (>40 Gy/s) have the ability to reduce the prevalence of negative side effects in patients without sacrificing tumor control. This study focuses on whether dose rate affects the degree of damage to healthy tissues caused by ionizing radiation. Understanding the biological mechanisms that influence the response to radiotherapy and specifically FLASH radiotherapy is therefore key knowledge in the development of new therapeutic protocols.

This study evaluates dose-rate effects using zebrafish embryos as a small model organism. To study dose-rate effects the zebrafish are irradiated at 24 hours post fertilization and biomarkers are researched to asses dose-rate effects. They are irradiated using a ^{60}Co irradiator providing a dose-rate of 0.015 Gy/s and a second one providing a dose-rate of 0.211 Gy/s. Several biomarkers for radiation damage are identified, including rate of embryonic development (hatching), DNA breaks and apoptosis. The DNA breaks are measured using a TUNEL assay and apoptosis through a caspase-3 assay. The results of the assay's are measured using confocal microscopy.

Monte Carlo simulations of the experimental setup were performed to assess the uniformity of radiation and effective dose. They show a homogeneous dose throughout the sample, they show a 37 % lower dose in water in the sample compared to air.

The hatching biomarker shows that the hatching rates are 0.24 ± 0.03 for non irradiated samples and 0.37 ± 0.31 and 0.43 ± 0.20 for samples that have been irradiated with respectively 0.008 Gy/s and 0.015 Gy/s with a total dose of 10 Gy. It shows that the hatching rates decreases for the irradiated embryos compared to the non irradiated samples however no significant difference can be found for different dose-rates. The sub-cellular biomarkers, the TUNEL assay and the caspase-3 assay, seem more promising in detecting dose-rate differences but more research is needed to find the dose-rate effects on DNA damage and apoptosis. In order to gain a fuller picture into the biological mechanisms of FLASH dose-rate radiation a greater variety of biomarkers and more research in to DNA damage and apoptotic biomarkers is needed.

Contents

Abbreviations

Abbreviation	**Full name**
Co	Cobalt
DNA	Deoxyribonucleic acid
dpf	Days post fertilization
DSB	Double stranded (DNA) break
ER	Endoplasmic reticulum
FLASH	Free Electron LAser Hamburg
gc200	Gamma cell 200 - ^{60}Co irradiator
Gy	Gray (unit - J/kg)
hpf	Hours post fertilization
HT50	50% of hatching time
IHC	Immunohistochemistry
LET	Linear energy transfer
MC	Monte Carlo
MCNP	Monte Carlo N-Paritcle
Ni	Nickel
RBE	Relative biological effectiveness
RID	Reactor institute delft
SF	Surviving fraction
TUNEL	Terminal deoxynucleotidyl transferase dUTP nick end labeling

1 Introduction

Radiation therapy has been one of the main treatments for cancer [46]. Though many patients can benefit from radiotherapy [37], a lot of negative side effects occur, like nausea, edema, skin irritation, trouble swallowing, fertility problems and fatigue [46]. In the search for less harmful treatments FLASH (Free Electron LASer in Hamburg) therapy shows promising results. FLASH therapy delivers the dose with a high dose-rate (>40 Gy/s), due to accelerated electrons [10]. A positive effect resulting from using high dose-rate radiation is called the "FLASH effect". This shows tissue sparing effects and reduced toxicity compared to conventional radiotherapy (>0.01 Gy/s) [19, 45, 61]. The first research on high dose-rate radiation has been conducted in the seventies [18, 44], and has recently been used as a stepping stone to investigate whether high dose-rate radiation could be beneficial clinically [6, 19, 20, 39, 40, 45, 61].

Recently zebrafish have been used to study the FLASH effects [7]. Zebrafish embryos are easy to use for research, they have been thoroughly investigated in the past [54] and their entire genome has been sequenced [13]. A study on the FLASH effect on zebrafish found no significant difference in survival, however it did show a significant difference in edema for a total dose of 25 Gy. Based on Gagnaire et al. [24], a difference in hatching time can also be observed for low dose radiation (>0.01 Gy/s).

In this thesis, exploratory research into the advantages of FLASH dose-rate radiation is conducted. In order to properly investigate FLASH effects a better understanding of the underlying biological effects is needed. In order to do so, a biological system is used: zebrafish. Zebrafish are a 3D multi-organ, living system of which the embryos allow for easy research. Understanding the underlying biological processes of the FLASH effect and, more generally, the biological effect of high dose-rate radiation will improve radiotherapy and contribute to curing more patients with minimal negative side effects. Therefore this thesis researches the following question:

What is the biological effect of high dose-rate ionizing radiation on Zebrafish compared to conventional radiotherapy?

This thesis will explore dose-rate effects and do exploratory research in the biological effects of different dose-rates. To gain more insight into different tissue responses to high dose-rate radiation. First the focus will be on the hatching rates of irradiated zebrafish. Later more sensitive, sub-cellular, biomarkers are used as biological endpoints: caspase-3 activity and TUNEL staing. Yabu et al. show that caspase activity and whole-mount TUNEL staining can be used to detect apoptosis [64]. These more sensitive biomarkers can provide more information on the biological effect of high dose-rate radiation.

The type of radiation available for this research is low dose-rate gamma radiation. Unfortunately that does not fall under the high dose-rate radiation range, however it can be used to observe dose-rate effects. The effective dose of radiation is verified using Monte Carlo dose calculations.

Chapter 2 provides the reader with background information about zebrafish, their development, and different biological experimental setups that can be done using zebrafish. Chapter 3 will explain some radiotherapy fundamentals, what is already known about the biological effects of radiation, and provide information about Monte Carlo dose calculations. In chapter 4 the specific methods and materials used in the experiments will be explained followed by the results. The simulation and experimental results will be shown in chapter 5. The last chapter will clarify and discuss the results and propose future steps for this research.

2

Zebrafish

Zebrafishes have been used in research for about sixty years now [54]. During this time researchers have manged to create many different lines of zebrafish each with their own investigative benefit. Some zebrafish lines have very little pigmentation, making them easier to image under a microscope. Others have been engineered to have fluorescent proteins encoded in their DNA allowing the researcher to analyze the expression of different genes under different conditions.

Using Zebrafish as a model organism in developmental studies helps gaining insight in the damaging effects of radiation and repair mechanisms in organisms. As a model organism, zebrafish have advantages over other organisms. The entire genome has been characterized and sequenced [13]. Zebrafish are vertebrate organisms which allow scientist to research structures and organs, some of their physiology is similar to humans, like a heart and a brain, other part diverge, like gills for example [63].

Zebrafish allow for easy study of the embryonic development because the embryo develops outside the mothers body and the embryos are transparent [14]. These features allow scientist to track the development in vivo on a cellular level. The fish also allow large-scale genetic studies because they spawn up to a hundred eggs every two to three days [17]. Besides the transparency and the large number of embryos, the embryos develop very fast, which is a very advantageous characteristic for research on many developmental, drug discovery and environmental impact studies [14, 56]. Most of the developmental processes of embryonic development of zebrafish are similar to those found in humans [14] resulting in more studies and new insights in DNA expression under different circumstances like radiological damage and developmental studies [24, 31, 35].

2.1. Developement

The developmental stages of zebrafish are categorized by the number of cells the embryo contains. Cell count can be used to accurately determine the phase the embryos is in during the undertaking of a study. They are visualized in figure 2.1.

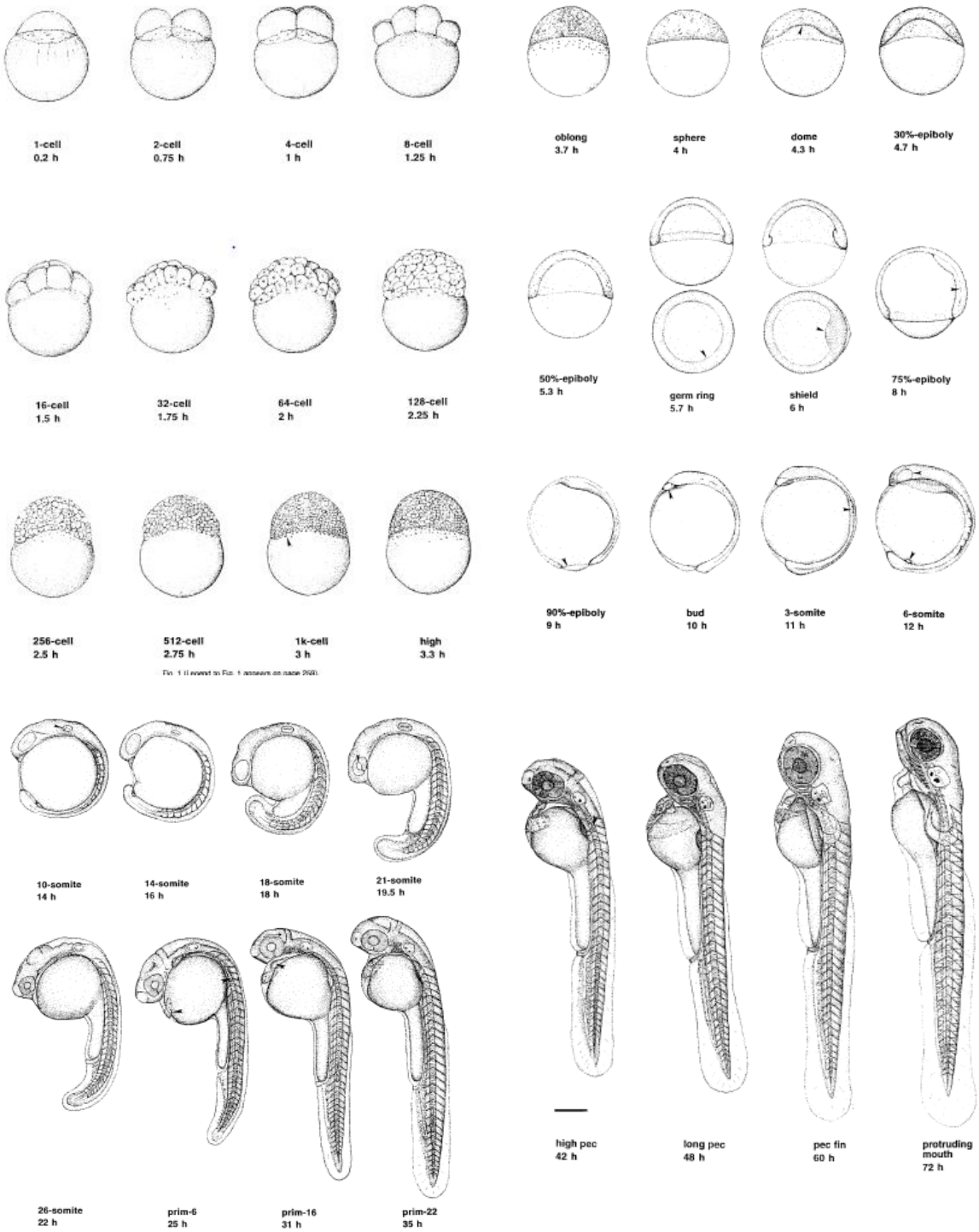

Figure 2.1: Stages of embryonic development in Zebrafish. Figure adapted from Kimmel et al. [38]

2.2. Microscopy experiments

Besides encoding fluorescent proteins in the DNA, different techniques can be used to localize a specific structure inside a cell. Immunohistochemistry (IHC) techniques use antibodies to bind fluorophores to specific sites of endogenous proteins, labeling them for visualization by light microscopy. The fluorophore can either be directly conjugated to a synthetic antibody (direct labeling), or a secondary antibody that has a fluorophore attached can be used to bind to the first antibody (indirect labeling). The advantage of IHC is that it is very specific and accurate. It results in very few false positives and false negatives. For this study the IHC method is used to detect the caspase-3 protein inside irradiated cells.

2.2.1. Caspase-3 assay

Caspase-3 IHC uses indirect IHC to visualize the amount of caspase-3 protein inside a cell. Caspase-3 is a biomarker for apoptosis as it is part of the caspase apoptotic pathway.

The caspase apoptotic pathway can be activated by intrisic or extrinsic signaling. Intrinsic signaling is induced by some for of cellular stress, like DNA damage or Endoplasmatic Reticulum (ER) stress. The stress activates proteins resulting in mitochondrial outer membrane proteins to be released. Cytochrome C binds to apoptotic protease activating factor 1 forming apoptosome. In its place apoptosome recruits caspace-9, strating a cascade ending in the activation of caspase-3 and caspase-7. The extrinsic pathway can directly activate caspase-3 and caspase-7 through the caspase-8 pathway. It can also indirectly activate caspase-3 and caspase-7 trough BID cleavage. [8]

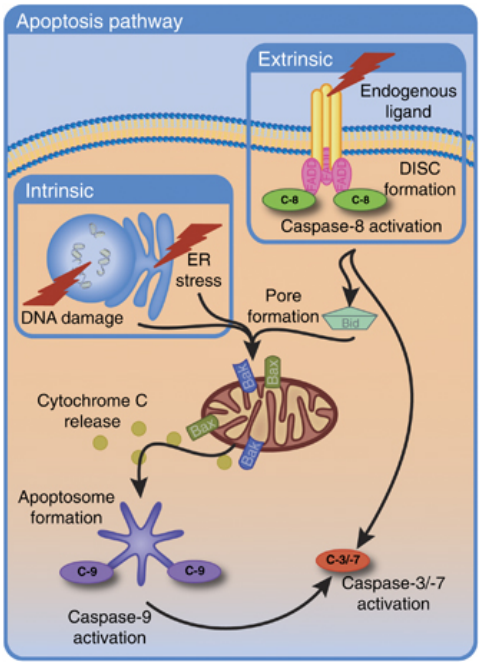

Figure 2.2: A graphical representation of the caspase apoptotic pathway [8]

The primairy antibody used in the caspase-3 IHC binds specificly to caspase-3. The seconairy antibody has a red flurophore attached to it and binds specifically to the primairy anti-body. This secondairy molecule can be localized using confocal imaging.

2.2.2. TUNEL assay

The biggest contributor to apoptosis is double-stranded DNA breaks. TUNEL staining can be used to detect DNA breaks, it uses a very similar technique to IHC were an enzyme, the TdT enzyme to be specific, binds to DNA breaks. It is a DNA polymerase that, in contrast to other DNA polymerases, does not need a template. It catalyzes the free 3'-hydroxyl ends of the fragmented DNA [1]. The enzyme binds to every free 3' -hydroxyl end of DNA, and therefor it binds to every DNA break. The TUNEL assay uses FITC as a flurophore. The FITC binds to the TdT and can therefor be localized the same way the secondary antibody can be localized in IHC. A TUNEL assay is used to detect DNA breaks.

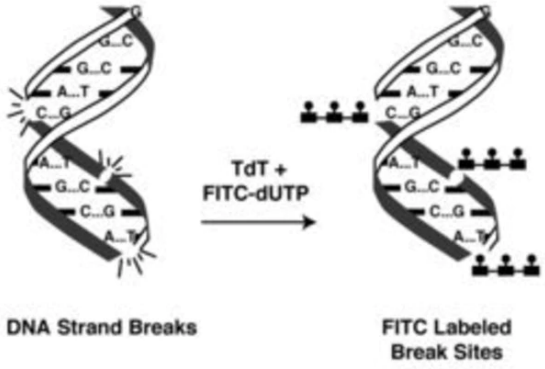

Figure 2.3: TUNEL staining labels the DNA breaks using TdT enzymes. FITC then binds to the enzyme resulting in a fluorescent molecule being bound to the enzyme. This way DNA breaks can be detected using a confocal microscope. Figure adapted from [53].

2.2.3. Confocal microscopy

A confocal microscope has five main components. There needs to be a sample with fluorophores to image, a laser to excite the fluorophores, a dichroic mirror to filter the excitation light from the emitted light, and a detector to capture the signal.

The working principle of confocal imaging is based on the absorption and emission of light by fluorophores. Fluorophores are molecules that absorb light in the visible spectrum. As the light is absorbed the molecules will be excited, and later released in the form of another visible photon. Fluorescent molecules can be attached to a particular protein or biological structure. This way a particular structure can be localized in the sample based on the emission of visible photons.

The difference in the absorption spectrum and the emission spectrum can be used to filter the signal. A dichroic mirror can be used to pass the specific wavelength of the emitted light. This way the scattered light used in the excitation of the sample will not reach the detector. The excitation light is usually a laser with a specific wavelength suitable for this sample. As a laser emits focused light, it can be used to excite a small part of the sample. Scanning mirrors are used to move the laser along the xy plane of the sample. This way the sample will be scanned. The Dichroic mirror, the sample, and the detector are shown in figure 2.4.

Another advantage of confocal imaging is that a pinhole can be used in order to filter out all the out-of-focus signal. Using the objective lens the light emitted from the focal plane of the sample will have the focal point right at the location of the detector. This light can go through the pinhole which is directly in front of the detector. Light emitted at a different plane will have a different focal point and will be stopped on the perimeter of the pinhole. The light will therefore not reach the detector.

In this research confocal imaging is used to localize the IHC fluorophores and the FITC fluorophore used in the TUNEL assay.

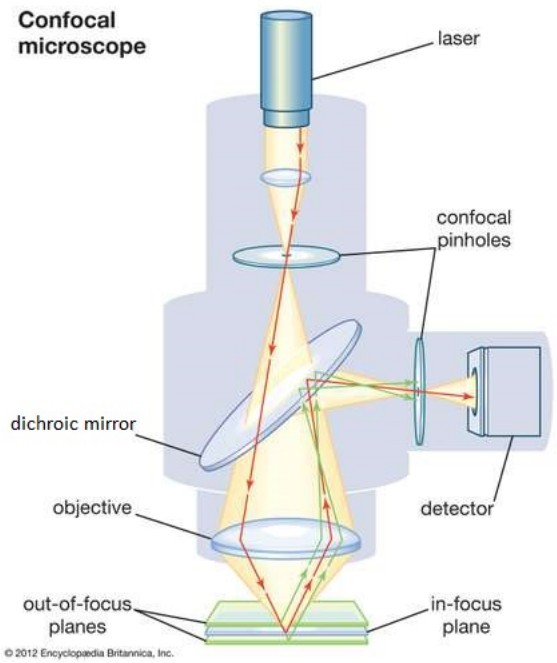

Figure 2.4: A confocal microscope uses a laser to excite a specific part of the sample. Inside the sample are fluorophores that absorb the energy of the laser. The emmited light by the fluorophores is then focused using the objective and filter using the dichroic mirror. The pinhole ensures that only the infocus light reaches the detector. [22]

3

Radiotherapy

Radiotherapy is defined by the National Cancer Institute (NCI) dictionary as: "The use of high-energy radiation from x-rays, gamma rays, neutrons, protons, and other sources to kill cancer cells and shrink tumors. Radiation may come from a machine outside the body (external-beam radiation therapy), or it may come from radioactive material placed in the body near cancer cells (internal radiation therapy or brachytherapy). Systemic radiotherapy uses a radioactive substance, such as a radiolabeled monoclonal antibody, that travels in the blood to tissues throughout the body. Also called irradiation and radiation therapy." [46]

As can be noted radiotherapy aims to kill as many tumor cells as possible using any type of radioactivity. For the purposes of this research only external beam radiation therapy is regarded, since external beam therapy is the most common radio-therapeutic treatment method. [2]

High energy radiation has a damaging effect on tissue in the form of ionization. When radiation interacts with the body it can damage the cells in two ways: by directly ionizing the DNA or by indirectly ionizing the DNA. In the latter case the radiation ionizes a compound resulting in a reactive species that in its place ionizes the DNA. When the DNA of a cell is irreparably damaged the cell will activate a process called apoptosis, programmed cell death. [36]

This chapter will provide a short overview on different radiation types and effects of radiation on tissues. More information can be found in "The physics of radiotherapy" by Khan [36] and "Inleidning tot de stralingshygiëne" by Bos et al. [9].

3.1. Types of radiation

When radiation interacts with a material, its energy can be absorbed by the tissue. How the energy is absorbed by the tissue depends on the properties of the radiation. With regard to external beam therapy there are two types of radiation: directly ionizing and indirectly ionizing radiation. Directly ionizing radiation are charged particles, like protons and electrons. Indirectly ionizing radiation is uncharged particles, like photons. Other relevant characteristics of radiation are the beam energy and the density of the material it interacts with.

3.1.1. Photons

Photon radiation has three prominent interaction types the photoelectric effect, the Compton effect and pair production. The photoelectric effect is the dominant interaction with lower energy photons. The photon is completely absorbed and in its place, an electron is ejected from the atom. The secondary particle had an energy lower than the energy of the photon, because of the binding energy of the electron. The Compton effect is a process in which only a partial energy loss for the photon is achieved. The incoming photon interacts with an electron and is emitted under an angle, reduced in energy, the electron is also emitted under a different angle having some energy from the photon. The last process is pair production in which the energy of a photon has to be greater than 1.022 MeV. During this process the photon loses all its energy in order to create one electron and one positron.

3.1.2. Charged particles

Charged particles directly ionize material as opposed to photons. Charged particles lose energy through ionizations and excitations. This results from the interaction between the Coulomb force between the traveling

particle and the material. The electric field of the traveling particle and electric fields of orbital electrons and nuclei of atoms of the material interact, resulting in a loss of energy. The energy deposition of charged particles increases when their energy is low. This is at the end of their range. The increase in energy loss at the end of the range is an important characteristic of charged particles, resulting in the so-called Bragg peak.

3.2. Radiation damage

Both direct and indirect ionization, can inflict damage to cells. The types of damage depends on the location of the energy loss. With respect to apoptosis the most important damage is double stranded DNA damage.

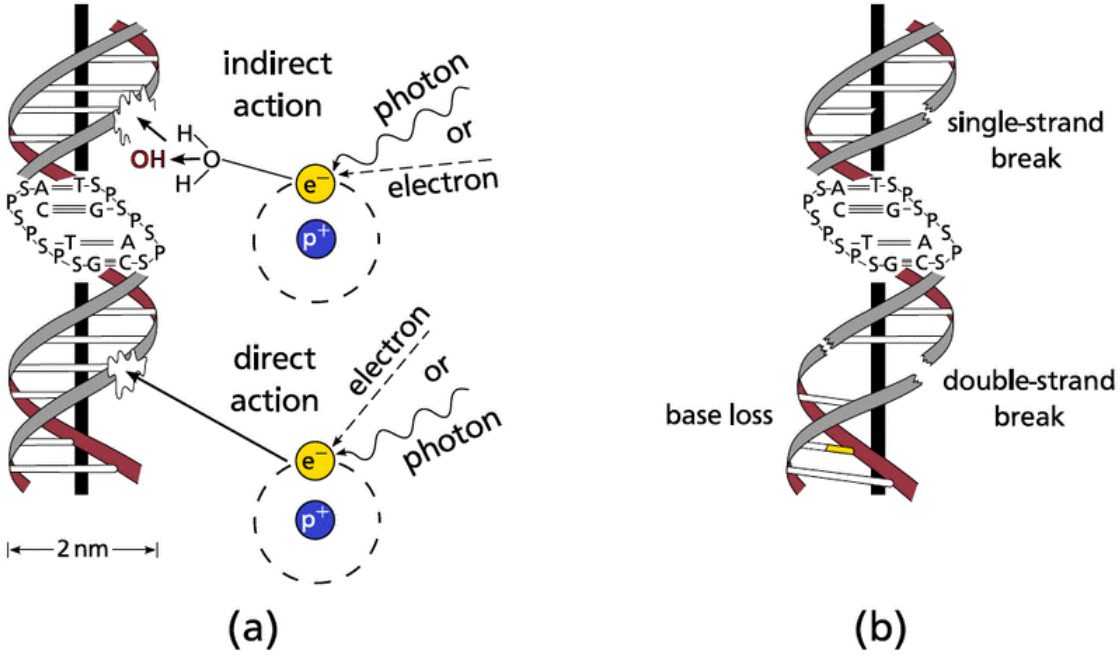

Figure 3.1: (a) Direct and indirect radiation damage. Direct DNA damage directly deposits its energy on the DNA molecule and damages it. Indirect damage is damage where the high energy radiation ionizes a particle that in turn damages the DNA. (b) Types of DNA damage. Double stranded damage is much harder to repair than single stranded DNA damage. Figure adapted from [28]

DNA damage occurs when high energy radiation loses part of its energy by interacting directly with the DNA molecule. As a result of this interaction a break in the DNA molecule occurs. A break in one side of the DNA helix is called a "single strand break". However, when close to the first break a second break to the other DNA strand takes place, it is called a "double-strand break" (DSB). As the chromosome is now completely broken it is more difficult for the cell's DNA repair mechanisms to repair the DNA in the proper manner.

DSB are dificult to repair, therefor mistakes in DNA repair occur frequently in DSB. When the DSB is not repaired properly the DNA chromatins can drift apart. Alternatively it can lead in an alteration of the junction. The most common repair mistake is called "translocation". In the case of translocation the ends of different chromosomes are joined together resulting in chromosome aberrations. [52]

The type of radiation influences the type of damage inflicted on a cell. Radiation with many interactions in a short range, like in the Bragg peak, have a higher chance of causing DSB. Therefore the radiation damage is not always proportional to the absorbed dose. The amount of energy transfered in the material over a certain distance is an important factor to include. Not all types of radiation will do the same type of damage. The amount of energy transferred into a material caused by ionizing particles of a specified energy in a traversing distance is defined as the linear energy transfer (LET) given by equation 3.1.

$$LET = \frac{dE_L}{dl} \tag{3.1}$$

Where dE_L is the energy loss and dl is the traversing distance of the charged particle. Depending on the type of radiation the LET can either be high or low. Photons have a low LET whereas charged particles have a higher LET. The different damages that types of radiation can do are visualized in figure 3.2.

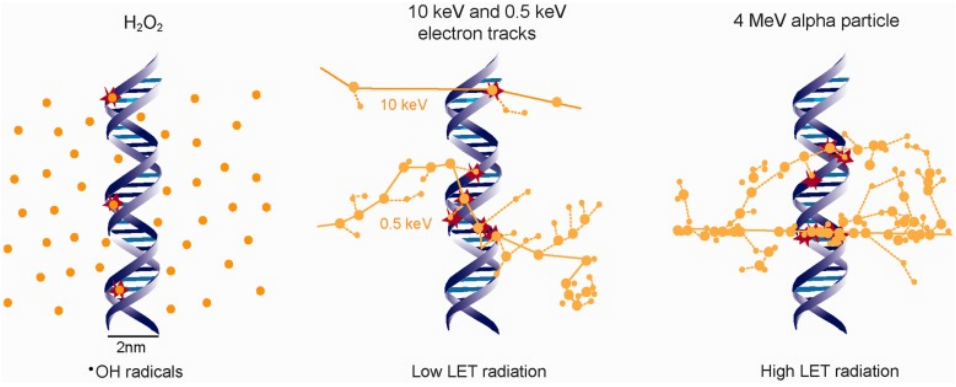

Figure 3.2: A visualization of DNA damage by different LET radiation [52]

3.3. Depth Dose curves

When radiation passes through a medium the dose attenuates depending on the density and the mass attenuation coefficient. Different radiation types and intensities attenuate in different ways. The depth dose curve is a way to visualize the absorbed dose in the medium. It is normalized to the maximum dose inside the medium.

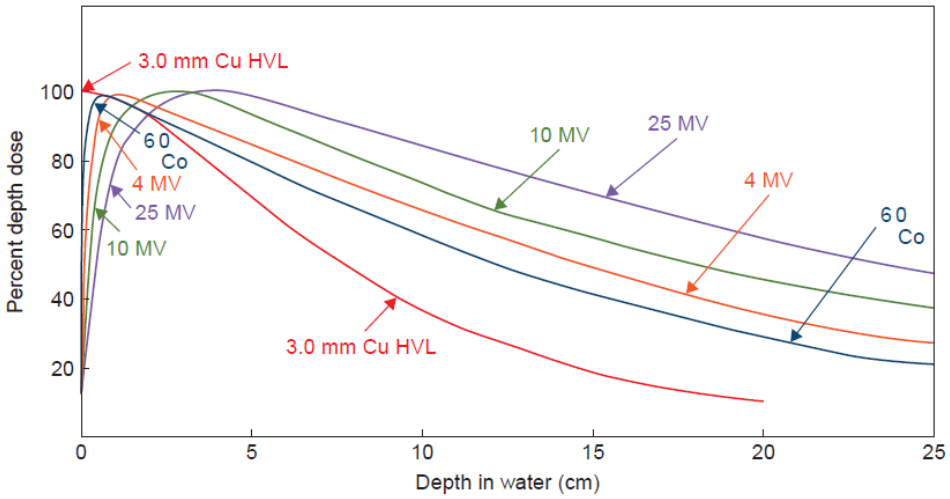

Figure 3.3: Depth dose curves of different types of radiation. The distance between the source and the surface of the medium is 100 cm for all beams except for 3.0 mm Cu half-value layer, that distance is 50 cm. The field size of the beam is $10x10cm^2$. This figure is adapted from [36] and uses data from [57].

The first region in figure 3.3, were the dose has not reached it maximum yet, shows the 'build up region'. It is the area were part of the dose scatters to the area outside the medium. Some particles do scatter inside the medium resulting in a higher dose in the next layer. Deeper inside the medium the particles scattered form other depths in that medium are the equal to the number of particles lost due to scattering. This results in a 'charged particle equilibrium'. When there is charged particle equilibrium the dose shows an exponential decay in accordance with 4.1.

3.4. Relative biological effectiveness

In order to be able to compare different types of radiation and different fractionation schemes, every type of radiation is compared to a reference radiation. The reference radiation often are the photons released by ^{60}Co radioactive decay or 250 keV X rays [36]. When the radiation results in more cell death compared to the reference radiation, a lower surviving fraction (SF), for the same dose the radiation is more effective and therefore has a higher relative biological effectiveness (RBE) [59]. The surviving fraction for each dose can be shown in dose-response curves, an example of a dose-response curve is shown in figure 3.4.

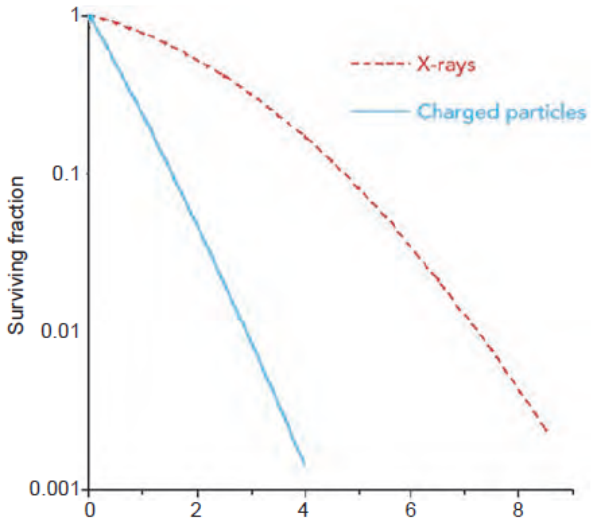

Figure 3.4: Surviving fraction as a result of X-ray radiation and charged particle radiation. [25]

The effect that a certain radiation dose has on the medium is often modeled by the "linear quadratic model". This model is used to express the SF for different radiation types shown in equation 3.2.

$$SF(D) = e^{-\alpha D - \beta D^2} \tag{3.2}$$

The SF of the medium depends on the total absorbed dose, D, and biological parameters α and β. α and β are depending on different factors like type of radiation, dose rate and cell type. α is often explained as sensitive to single track damage and β as sensitive to two independent tracks. The linear quadratic model does not include any repair.

The RBE compares biological endpoints, like the SF of the medium to the reference radiation. It compares the X-ray dose needed under the same conditions to produce the same endpoint [59]. The RBE can be expressed by the following formula:

$$RBE = \frac{D_x}{D} \tag{3.3}$$

where D_x is the X-ray dose and D is the dose needed to reach the same biological effect.

In the case of charged particles the RBE is not constant over the entire course of the particle track, as the particles slows down and the number of interactions increase. This results in an increased RBE in the Bragg peak.

3.5. Fractionation

It is not just the radiation type that influences the biological effectiveness. Another factor that influences the RBE is the number of fractions the dose is divided in and how far apart those fractions are. In the clinic, the time between fraction is usually 24 hours, as patients return to the hospital every day. An example of what the dose-response would be to a fractionated irradiation treatment, is shown in figure 3.5.

Giving multiple fractions ensures that more tumorous cells are killed. The reason for this is that some cells are in a more radio-resistant phase. If some time has passed the cells could be in a more sensitive phase resulting in a higher biological effectiveness. Aside from radiosensitivity, repair also plays a rol, as healthy cells are quicker and better to repair damage than tumor cells. As a result the linear quadratic model, formula 3.2, needs to be adapted to account for fractionation. The formula will be adapted to account for the dose per fraction. The total dose can be defined as n times the fraction dose, d; resulting in $D = nd$. Using this information the linear quadratic model can be adapted to [43]:

$$SF(D) = e^{-n(\alpha d + \beta d^2)} \tag{3.4}$$

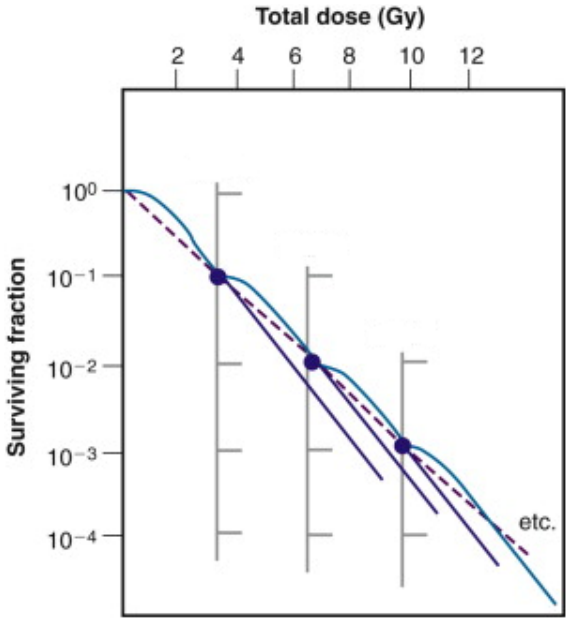

Figure 3.5: Fractionation effects [65]

3.5.1. Five R's of radiotherapy

There are five processes on a cellular level that change the effectiveness of radiotherapy. The first four are repair, repopulation, redistribution and reoxygenation [62]. Repair of sublethal injury means the repair of DNA and important proteins within the cell. Repopulation of cells means that tissues will regenerate after damage. Redistribution through the cell cycle means that the cells will get in different cell cycles, some of which will have more beneficial cell cycles in terms of radiotherapy. Reoxygination of the tissue means that the oxygen depleted cells will have time to get more oxygen; especially the cells deeper inside the tumor will have a chance to reoxygenate. [62]. The fifth factor added was radiosensitivity, which can be described as the difference in sensitivity to radiation between different cell types [5].

As explained in section 3.2 the cell has repair mechanisms that can repair DNA damage, especially single strand DNA damage. Cells find themselves in different stages of cell division. There are four stages in a cell cycle, G1,S,G2 and M. The cells are the most radiosenstive when the DNA is exposed. During the cell division, the M-phase, the DNA is less tightly bound in order to be able to duplicate it leading to the highest radiosensitivity. Mostly tumor cells respond quickly to a reduction in cell population by dividing even quicker and repopulate the irradiated area. Normal tissue cells have a slower response and repopulate later [59]. Oxygen is turned in to a radical as a consequence of ionization, inflicting even more harm to cells. As tumors are usually hypoxic due to reduced vascularization, reoxygenation increases the radiosensitiviy in tumor cells.

3.6. Cobalt decay

$^{60}_{27}$Co is a nuclide used in medical research. ^{60}Co has 27 protons and 33 neutrons, the half life is about 5.27 years [34]. It decays through beta decay to $^{60}_{28}$Ni and releases two gammas of 1.1 and 1.3 MeV [34]. The decay scheme follows the process displayed in: equation 3.5.

$$^{60}_{27}\mathrm{Co} \longrightarrow {}^{60}_{28}\mathrm{Ni} + \mathrm{e}^- + \overline{\nu}_e + \text{gamma rays} \tag{3.5}$$

^{60}Co barely occurs naturally [33] and is mostly used for industrial and medical purposes, like sterilization of medical equipment. It is man made using neutron activation in a nuclear reactor. ^{59}Co absorbs a neutron and is converted in to ^{60}Co:

$$^{59}_{27}\mathrm{Co} + {}^{1}_{0}\mathrm{n} \longrightarrow {}^{60}_{27}\mathrm{Co} \tag{3.6}$$

^{60}Co is produced in a nuclear reactor by placing pellets of ^{59}Co inside the reactor. A small percentage of the atoms then absorbs a neutron resulting in ^{60}Co. The pellets are than encapsulated in material that

allows the radiation to penetrate but not the material itself. The pencils can than be placed in the desired configuration inside a source. [33]

The reactor institute in Delft contains one of these ^{60}Co sources: the gc200 from the Atomic Energy of Canada Limited. It has a dose-rate of 0.015211 Gy/s in March of 2019. The source consist of 24 of these ^{60}Co pencils placed around a sample chamber.

3.7. Monte Carlo simulations

The dose-rate of the gc200 is measured in air in the middle of the sample chamber. As it can be challenging to place the sample precisely in the middle of the sample chamber and not all samples can be irradiated in air, Monte Carlo calculations can be used to accurately calculate properties of radiation. Different properties can be dose-rate, total dose and difference between media.

Monte Carlo calculations use random numbers to calculate the path and interaction of every particle. As explained above photons attenuate when they travel through a medium. As a result every individual photon interacts on a different distance from the source and deposits a different amount of energy. Monte Carlo calculations calculate these properties for every single photon and its secondary particles until that photon is completely absorbed. In order to be able to calculate all of these interactions the probabilities of all of these interactions need to be known.

Monte Carlo simulations simulate a sample of a population of possibilities. When the sample is random enough it tends to exhibit the same properties as the entire population. In order to confidently predict the properties of the population the sample size needs to be larger when dealing with a large variance. The goal is to get a result with a variance small enough to confidently determine the behaviour of the population. [27]

In our case we use Monte Carlo simulations in order to simulate individual particles to get an estimation of the dose in our sample. The location, the energy and the direction of the particle is chosen randomly by the code from known probability distributions. The probability of a certain energy is given by the user, in our case 1.1 and 1.3 MeV, as it depends on the energy of the material in a specific problem. In order to calculate the interaction of each individual particle both the path length and the type of interaction is sampled. The path length and the type of interactions determine the dose deposition in the surroundings. The path length is calculated using the attenuation coefficient, which is depended on the type of the material and the energy of the radiation. All these parameters are sampled from known probability distributions using a random number generator. The sampling from a known distribution is the basis of the Monte Carlo calculations. [60]

The code used in this research is the MCNP code, a general purpose Monte Carlo N-Particle code developed by Los Alamos National Laboratory [3]. It was originally developed for neutron-photon transport, used in reactor calculations. Nowadays it can be used for neutron, photon and electron transport or any type of coupled transport between these [3]. It has a powerful geometry package and can be adapted to medical physics purposes [51].

4

Methods and Materials

4.1. Experimental conditions

Zebrafish embryos were obtained by breeding adult zebrafish. Adult fish were maintained in 3 liter tanks at 28 °C on a 14/10 light-dark cycle with a maximum of 20 fish per tank. The system water was constantly pumped, filtered and kept sterile using UV-light. The conductivity, hardness and pH of the water were monitored and always within the acceptable range. The fish were fed twice per day with a combination of live artemia and GEMMA micro dry food. The artemia were raised for 24 hours in salt water with air bubbles. The fish were checked once a day to monitor their health.

4.1.1. Crossing and collecting

Experiments were conducted on embryos within five days past fertilization (dpf). Embryos were obtained by crossing one pair of fish per crossing tank. Crossing tanks are normal tanks in which an extra holder is placed containing a false bottom. In this case the eggs will fall to the bottom and can be collected without disturbing the fish. It also ensures the maximum amount of eggs as they can not get eaten by the adults.

Figure 4.1: Example of a breeding tank used for crossing adult fish

Crossings are set-up at night and are collected in the morning. The embryos are then plated with a maximum density of 100 embryos per petri dish. They are immersed in egg water (system water + with methylene blue). The adult fish used for breeding were of the wild type (AB), the casper type and the MPEG:gfp fish which have an AB background.

The embryos are transported to the irradiation location at the Reactor Institute in Delft (RID) location. The fish are transported in falcon tubes inside a cardboard box filled with tissues to ensure minimal shaking (mechanical disruption). The carboard box is placed inside a styrophome container to ensure that the fish remain as warm as possible. When in the reactor builing the embryos were place in small petri-dishes that are

placed inside the irradiator. For the transport back they were moved back in to the falcon tubes, carboard box and styrophome box and transported back to the fish room. In the fish room they were place in normal petri dishes at a density of maximum 100 fish per petri dish. The fish were monitored for morphological changes at intervals of 30 minutes to 1 hour during the day and whenever possible during the night.

4.2. Hatching assay

Embryos were irradiated with gamma rays at 24 hours post fertilization (hpf). With a dose-rate of 0.015 Gy/s at the gc200 or a halved dose-rate of 0.008 Gy/s achieved by adding lead shielding around the sample. The hatching was monitored afterwards to see the effect of different total doses and different dose-rates. Three different variables were investigated to see their influence on hatching. The first variable is to see is when in their development they receive their radiation has an effect on hatching. The second variable is to see how total dose influences the hatching and the third is the actual variation of the dose-rate. For each of the experiments the time that 50% of the embryos have hatched (HT50) is shown for each of the hatching curves. The HT50 will always be given in hpf.

4.2.1. Time of irradiation

The embryos were born at 9 am and were irradiated 24 hpf, 27 hpf and 30 hpf the next day. A timed cross was attempted to have two different ages at the time of irradiation. At a timed cross the fish are put in the same tank 2 hours after the lights are on, instead of putting them together the night before. As a result the embryos of the timed cross will at least be two hours older. However the timed crossing did not succeed. For irradiation they were transported to the RID in the cardboard styrofoam box construction and a control group was also included. As the irradiation takes place in the dark the control group was kept in the dark for the entire irradiation time. The embryos received a total dose of 5 Gray.

4.2.2. Total dose

To investigate dose-effects the embryos were irradiated with 5, 10 and 20 Gy at 24 hpf in the gc200. The embryos were irradiated ate the RID and a control was taken. The embryos were moved in styrofoam box to control the temperature and in a cardboard box to limit the movement of the falcon tubes. The irradiation time of 10 Gy was double the time of five Gy and the irradiation time of 20 Gy was double the time of 10 Gy. After irradiation the hatching was monitored.

The eye development, tail curvature and level of edema were noted, however no images could be taken at the time so no quantitative metric could be used.

4.2.3. Dose-rate effects

The embryos were irradiated at 24 hpf with two different dose-rate. One group was irradiated inside the gc200 another group was irradiated inside the gc200, however the dose-rate was halved by placing a lead shielding around the petri dish. Their dose-rates are respectively 0.015 Gy/s and 0.008 Gy/s. The time of irradiation was therefor not constant. The embryos were irradiated at the RID and a control was taken. The embryos were moved in styrofoam box to control the temperature and in a cardboard box to limit the movement of the falcon tubes.

Qualitative variations in eye development, tail curvature and level of edemia were noted manually.

Two experiments have been conducted and are compared using a weighted mean comparison.

4.3. Staining

4.3.1. IHC

A short experiment using anti-GFP IHC was conducted to practice the technique. The results show good penetration and specificity. That suggest that the protocol and specifically the permeabilization steps work well.

For the anti-caspase-3 experiments the embryos crossed and collect according to normal procedures described in section 4.1.1. They were irradiated at 24 hpf with a total dose of 15 Gy. The dose-rate was 0.015 Gy/s for the first group and and 0.211 Gy/s for the second group. A control was taken to the RID as well to expose the embryos to the same level of temperature variation and mechanical disruptions. The embryos were fixated at 30 hpf and 3 days post fertilization (dpf) in 4% para-formaldehyde (PFA). The embryos were permeabilized using pronase before PFA fixation and collagenase before the staining procedure. The pronase

incubation was used as dechorionation procedure for the 30 hpf embryos by swirling the eppendorfs during the 10 minute pronase incubation with a concentration of 10 mg/ml system water. The 3 dpf embryos were incubated in a 2 mg/ml eggwater solution for 10 minutes. The 30 hpf embryos were incubated in 0.2% collagenase in PBS for 20 minutes and the 3 dpf were incubated in 0.2% collagenase in PBS for 60 minutes, as a final step of permabiliztion.

The primairy Anti-Caspase-3 antibody was obtained from abcam (ab13847) and was used in a PBSTw + goat serum buffer solution, the dilution was 1:500 mM overnight at 4°C. The secondary antibody is a donkey Anti-Rabbit IgG H&L (Alexa Fluor® 647) and is obtained from abcam (ab150075). The the secondary was incubated in the same buffer solution with a dilution of 1:400 for 4 hours on a rocking platform at room temperature.

The same embryos were diluted in DAPI staining with a dilution of 1:5000. The 30 hpf group is incubated for 20 minutes and the 3 dpf group is incubated for 60 minutes.

For both TUNEL staining and immunostaining there were four groups. The first group is the "Staining control" group, it did not receive the primairy anti-body or the TdT enzyme, respectively in IHC and TUNEL staining. This group is to check if the signal results from the binding to the relevant biomarker. The second group is the "radiation control" group, this group did not receive any radiation and will serve as a negative control. The last two groups did receive a radiation dose of 15 Gy with a dose rate of 0.211 Gy/s and 0.015 Gy/s. For IHC a positive control was provided by inducing endoplasmatic reticulum (ER) stress using thapsigargin, shown in figure 4.2; ER stress induces apoptosis. The thapsigargin was used in concentrations of 2 µM and 20 µM. Table 4.1 gives a schematic overview of the groups.

After staining, the embryos were kept in a PBS buffer and either mounted in glycerol or 2% agarose and imaged using a confocal microscope.

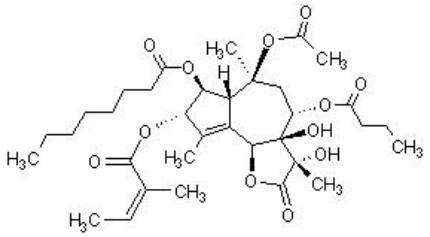

Figure 4.2: Molecular structure of Thapsigargin

To understand the effectiveness of thapsigargin one assay of 2 mM was executed to identify the amount of embryos that survived. Therefor the thapsigargin group is not included in the data analysis and the results.

Table 4.1: Schematic display of the properties of the different staining groups

	Radiation	**Conjugate to biomarker present**
Staining control	No	No
Radiation control	No	Yes
15 Gy, 0.211 Gy/s	Yes	Yes
15 Gy, 0.211 Gy/s	Yes	Yes

4.3.2. TUNEL

The embryos crossed and collect according to normal procedures described in section 4.1.1. They were irradiated at 24 hpf with a total dose of 15 Gy. The dose-rate was 0.015 Gy/s for the first group and 0.211 Gy/s for the second group. A control was taken to the RID as well to expose the embryos to the same level of temperature variation and mechanical disruptions. he embryos were fixated at 30 hpf and 3 days post fertilization (dpf) in 4% PFA. The embryos were permeabilized using pronase before PFA fixation and collagenase before the staining procedure. The pronase incubation was used as dechorionation procedure for the 30 hpf embryos by swirling the eppendorfs during the 10 minute pronase incubation with a concentration of 10 mg/ml system water. The 3 dpf embryos were incubated in a 2 mg/ml eggwater solution for 10 minutes. The 30 hpf embryos were incubated in 0.2% collagenase in PBS for 20 minutes and the 3 dpf were incubated in 0.2% collagenase in PBS for 60 minutes, as a final step of permabiliztion.

The TUNEL staining kit was obtained from abcam (ab66108). The concentrations used were according to the abcam protocol. Using TdT, FitC in a reaction buffer diluted with MilliQ water. The 30 hpf embryos were incubated for 1 hour in 37 °C and the 3 dpf embryos were incubated for 2 hours in 37 °C.

The same embryos were diluted in DAPI staining with a dilution of 1:5000. The 30 hpf group is incubated for 20 minutes and the 3 dpf group is incubated for 60 minutes.

After staining the embryos were kept in a PBS buffer and either mounted in glycerol or 2% agarose and imaged using a confocal microscope.

4.3.3. Data processing

The confocal images collected on the microscope are exported and analyzed with the ImageJ software suite (NIH). Unfortunately the images were recorded at 16 bit, but exported as 12 bit images, so they are all caped at 4095. Each color channel was analyzed separately. For z-stacks, each image plane was analyzed separately. Images were first thresholded to filter out the background. Then a bitwise AND operation is conducted to compare the signal in the two stacks. A maximum projection is made for visualization purposes and a measurement of the intensity of the pixel values is made in each slice of the stack. This way the signal intensity of the DAPI staining and the histochemistry staining is compared.

4.4. Monte Carlo dose calculations with MCNP

Monte Carlo calculations are used to ascertain an approximation of the dose inside the zebrafish. A model of the gc200 is built using MCNP software. The software used is MCNP version 6.2 produced by Los Alamos National Laboratory in the United States and it allows to track many particle types over broad ranges of energies [3].

MCNP has three main inputs: the cell cards, the surface cards and the data cards. Cell and surface cards determine the geometry, data cards regard particle type, material specification, source specification, tally specification and problem termination.

4.4.1. General information about the gc200

Some information is already known about the gc200 from the user manual. This information is important to know in order to specify the geometry and the source and to verify the results. The geometry (section 4.4.2) and the isodose lines throughout the sample chamber are documented. It is important to realize the position the sample is placed inside the chamber as the difference in dose can be significant.

4.4.2. Geometry of the gc200

One of the most important things when building the simulation is defining the geometry. The code is built in steps starting from a simple cylindrical geometry with a point source in the middle building up to simulated geometry of the gc200. The gc200 is modeled using the dimensions from the manual [3].

The dimensions of the gc200 are based on the dimensions as specified in the manual. Figure 4.3b shows a schematic representation from the manual of the properties of the gc200.

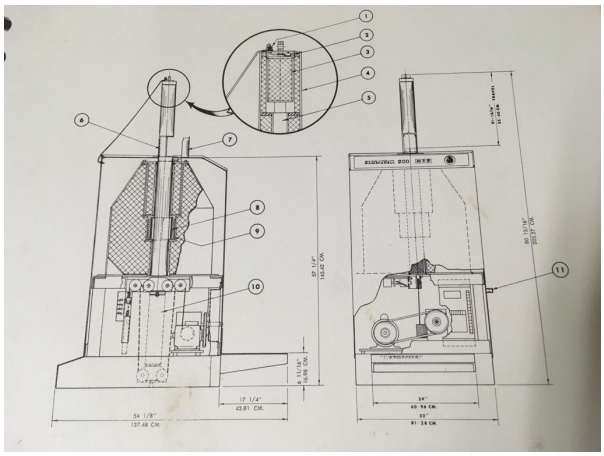

(a) Geometry specifications of the gc200

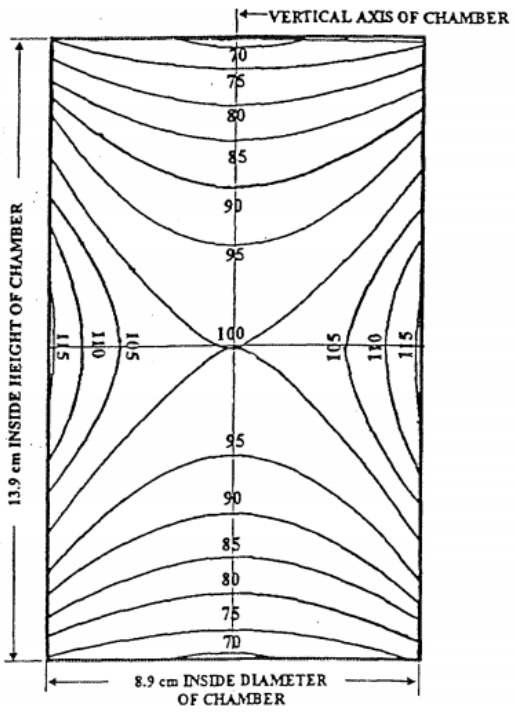

(b) Isodose lines inside the gc200 sample chamber. Obtained form [55]

Figure 4.3: Specifications of the gc200 ^{60}Co irradiation source used in experiments and simulations

Cylinder

The first step in building a model was to have two cylinders. The outside of the outer cylinder will be void. The middle part will be water and the outer part will be cobalt, figure 4.4.

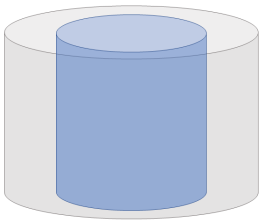

Figure 4.4: Simple model of the gc200. The grey outside cylinder shows the ^{60}Co, the blue inside cylinder shows the cylinder consisting of water.

Cylinder and pencil

The geometry of the gc200 consist of 24 ^{60}Co pencils. The first step in building the models to include one pencil in the middle of the geometry, see figure 4.5. The inside cylinder will model the sample chamber.

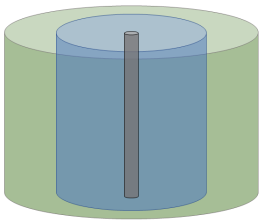

Figure 4.5: The green shows the air around the sample chamber. The blue is the water inside the cylinder. The grey shows the ^{60}Co pencil.

Four pencils on the side

In order to get more similar to the actual geometry of the source four pencils are places on the outside of the sample chamber. These four pencils are 90 degrees apart and on 6.1 cm from the center.

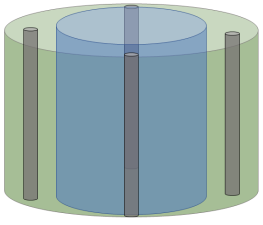

Figure 4.6: The four pencils are placed outside the sample chamber. The green represents air, the blue represents water and the grey represents ^{60}Co. There is one pencil in the front, one in the back, one on the left side of the sample chamber and one on the right.

24 pencils around the sample chamber

As a last step to complete the geometry of the source itself 24 pencils are placed around the sample chamber. These pencils are place with a distance of 6.1 cm from the center and are evenly spaced around the sample chamber.

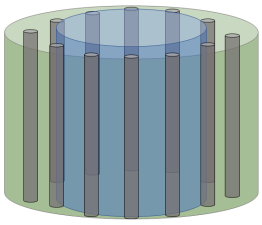

Figure 4.7: 24 ^{60}Co pencils evenly distributed around the sample chamber. The green represents air, the blue represents water and the grey represents ^{60}Co. This images only depicts 12 pencils for visualization purposes, however in the simulation 24 pencils are placed around the sample chamber.

4.4.3. Physics mode

The Physics mode is set to photons and electrons as ^{60}Co decay results in 1.3 MeV and 1.1 MeV photons [34]. Those photons create electrons when interacting with a medium. Therefor the physics mode is set to both photon and electron transport.

4.4.4. Source definition

Using the original certificates as starting point for the decay of the pencils the current activity is calculated using formula 4.1.

$$A(t) = A_0 * e^{\frac{-ln(2)*t}{t_{1/2}}} \tag{4.1}$$

The measurement time at the certificates was 25 Februari 1983 and as current time 7 June 2019 is used.

In order for MCNP to correctly sample all the right initial energy and direction the input requires the starting position inside the pencil, which pencil and the energy of the particle. As the pencils are cylindrical the starting position of the particles will be uniformly sampled over the radius and the height of the cylinder. For every pencil, modeled by a cylindrical cell, the cell position is defined by the coordinates of the base of the cylinder. Which pencil it starts is sampled from the ratio derived from the activity calculations. The starting height and radius are sampled separately and the energy of the particle will be evenly sampled from 1.173 and 1.332 MeV.

The simulations were started with two different seeds. This way it was checked if the initial seeding has an influence on the outcome of the simulation.

4.4.5. Materials

The materials used in the MCNP code are: air, water, lead, plastic, ^{60}Co and agar. They are introduced into the code by adding the atomic fractions of each material. The density of the material is introduced for every cell. The exact atomic fractions used in this problem can be found in Appendix B.

Our sample contains a petri dish, consisting of plastic, with water or agar (2% in water) inside surrounding the embryos. The dose-rate inside is compared for an empty petri dish, one filled with water and one filled with agar. The material and the density is adapted to the specific cases in the cell. The density of agarose is measured experimentally using a falcon tube to determine the volume and a scale to determine the weight. The density was $1 g/cm^3$. It would however be likely that the density would be a higher, unfortunately this method was not precise enough to measure that.

4.4.6. Tally

In order to measure the results of the radiation a tally is used. In our case the tally used to calculate the dose-deposition inside the petri-dish is the F6 tally. It measures the dose-depostion per starting particle in MeV/g. The F6 tally assigned to both photons and electrons. A +F6 tally is assigned to calculate the total dose resulting form all the particles created in the simulation. To asses the dose-deposition at different locations, inside and outside the petri-dish, an FMESH tally is used. It measures the dose-deposition per voxel, the voxel size can be assigned by the user and depends on the size of the mesh.

The dose can be compared to the measured dose at the quality assurance measurements, where the dose is measured in Gy/s. In convert the dose from MeV/g to Gy/s, a conversion factor is used.

$$\begin{aligned} 1 MeV/g \times 1{,}602 \cdot 10^{-13} J/MeV = \\ 1{,}602 \cdot 10^{-13} J/g \times 10^{3} g/kg = \\ 1{,}602 \cdot 10^{-10} J/kg \end{aligned} \tag{4.2}$$

The MCNP output for the FMESH can only be given in flux. In order to obtain the dose deposition a multiplier is used for the photon FMESH. This multiplier depends on the atomic fraction, the material, the total photon cross sections and the total photon heating. This multiplier is based of Diedrick Feilzers work [21]. For the electron FMESH tallies the electron stopping powers are used as mulitpliers.

As all of the dose is deposited by secondary particles it is important to note how MCNP handles just photon transport. MCNP regards the first interaction of the photon; if the interaction creates a secondary particle it will not be tracked. The dose will be deposited at the position of the interaction.

4.5. Tally verification

To check if the the tallies work properly a point source is placed in a pool of water. The pool will be made big enough to ensure no radiation escapes. This can be used to check if the total energy in the system, measured by the tallies is consistent with the total energy put in to the system. The pool has the dimensions of 10m x 10m x 10m. 100 photons with an energy of 1.1 MeV are simulated in photon mode and the coupled photon electron mode. The tallies are the same tallies used in the ^{60}Co simulation, these are: F6:P, F6:E, +F6 and FMESH:P and FMESH:E. So they are absorbed dose tallies and mesh flux tallies using a conversion to dose tallies. The tallies are counting the entire system and none of the photons are lost due to the size of the pool.

When the result of the F6 tallies is multiplied with the mass and the number of photons used in this experiment the result should be equal to the amount of energy put into the system. The results are shown in table 4.2 and 4.3.

Table 4.2: Total amount of energy measured in the system in photon mode

	+F6	**F6:P**	**F6:E**	**sum over FMESH:P**	**sum over FMEHS:E**
Output (MeV/g)	$9.98 * 10^{-10} \pm 0.0578\%$	$9.98 * 10^{-10} \pm 0.0578\%$	$0 \pm 0\%$	$9.75 * 10^{-2} \pm 4.8 * 10^{-4}\%$	$0 \pm 0\%$
Total MeV in system	99.8 ± 5.8	99.8 ± 5.8	0 ± 0	97.5 ± 0.05	0 ± 0

Table 4.3: Total amount of energy measured in the system in coupled photon electron mode

	+F6	**F6:P**	**F6:E**	**sum over FMESH:P**	**sum over FMEHS:E**
Output (MeV/g)	$1.10 * 10^{-9} \pm 0\%$	$1.02 * 10^{-9} \pm 0.0588\%$	$1.10 * 10^{-9} \pm 0\%$	$9.83 * 10^{-2} \pm 4.7 * 10^{-4}\%$	$1.3 * 10^{-3} \pm 3.5 * 10^{-4}\%$
Total MeV in system	110 ± 0	101 ± 5.8	110 ± 0	98.3 ± 0.05	$1.28 \pm 4.4 * 10^{-4}$

In table 4.3 the tally results show that the electron tally and the total dose tally correctly tally all the energy in the system. However when looking at the electron mesh values is 1.28 MeV for the calculation of the total energy in the system. However the total energy put into the system in this simulation was 110 MeV. This means that the electron mesh does not correctly tally the dose deposition. This could result from the kerma to dose conversion or MCNP doesn't tally all the dose deposition in the electron tally to begin with. However it is not known what the exact problem is.

5

Results

5.1. Monte Carlo simulations

The most important output from MCNP is the dose-deposition inside the petri-dish. Table 5.1 shows the results of the tallies, both photon and electron tally results and the +F6 tally which calculates the dose deposition of all the particles used in this particular problem. The code used to obtain these results can be found in appendix B. The code has been run twice with a different seed in order to check if the starting number influences the results of the simulation. The first seed is represented by water, air and agar, the second seed is represented by water2, air2 and agar2.

Table 5.1: Dose depostion inside the petridish for different content

Gy/s	**Total**	**Photons**	**Electrons**
water	$1.25 \cdot 10^{-2} \pm 1.06 \cdot 10^{-4}$	$1.08 \cdot 10^{-2} \pm 3.14 \cdot 10^{-5}$	$1.25 \cdot 10^{-2} \pm 1.06 \cdot 10^{-4}$
water2	$1.22 \cdot 10^{-2} \pm 1.05 \cdot 10^{-4}$	$1.09 \cdot 10^{-2} \pm 3.17 \cdot 10^{-5}$	$1.22 \cdot 10^{-2} \pm 1.05 \cdot 10^{-4}$
air	$1.98 \cdot 10^{-2} \pm 4.28 \cdot 10^{-4}$	$1.01 \cdot 10^{-2} \pm 2.74 \cdot 10^{-5}$	$1.98 \cdot 10^{-2} \pm 4.28 \cdot 10^{-4}$
air2	$1.93 \cdot 10^{-2} \pm 5.00 \cdot 10^{-4}$	$1.02 \cdot 10^{-2} \pm 2.76 \cdot 10^{-5}$	$1.93 \cdot 10^{-2} \pm 5.00 \cdot 10^{-4}$
agar	$1.25 \cdot 10^{-2} \pm 9.60 \cdot 10^{-5}$	$1.09 \cdot 10^{-2} \pm 2.94 \cdot 10^{-5}$	$1.25 \cdot 10^{-2} \pm 9.60 \cdot 10^{-5}$
agar2	$1.22 \cdot 10^{-2} \pm 9.54 \cdot 10^{-5}$	$1.10 \cdot 10^{-2} \pm 2.96 \cdot 10^{-5}$	$1.22 \cdot 10^{-2} \pm 9.54 \cdot 10^{-5}$

Table 5.1 shows that the dose in water is about 37% lower than the dose in air. The dose-in agarose is also 37 % lower than the dose in air. The simulated dose in air of 0,020 Gy/s is higher than the dose measured for quality assurance, which was measured at 0,015 Gy/s.

5.1.1. FMESH results

The results are shown in MESHes to gain insight in the distribution of the dose inside the petri dish. For every mesh the middle slice in y is taken and shows the xz plane. Over the width and depth of the petri dish the average is taken in order to show the change in dose over the height and width. As mentioned before the exponential decay will decrease the dose towards the middle and the skin sparing effect will decrease the dose at the edges of the medium.

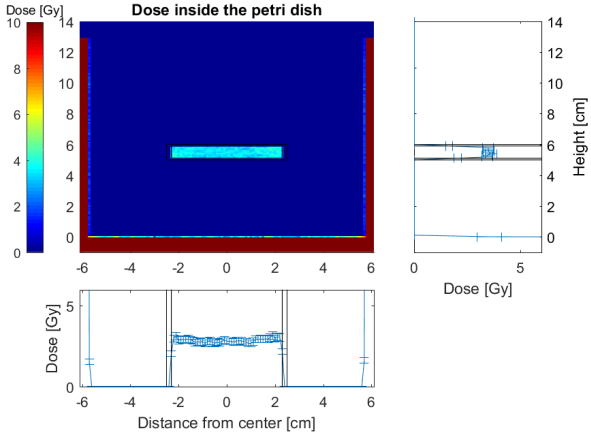

(a) Water

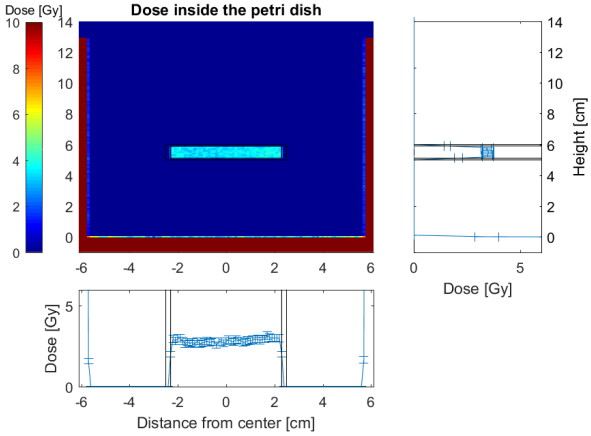

(b) Water 2

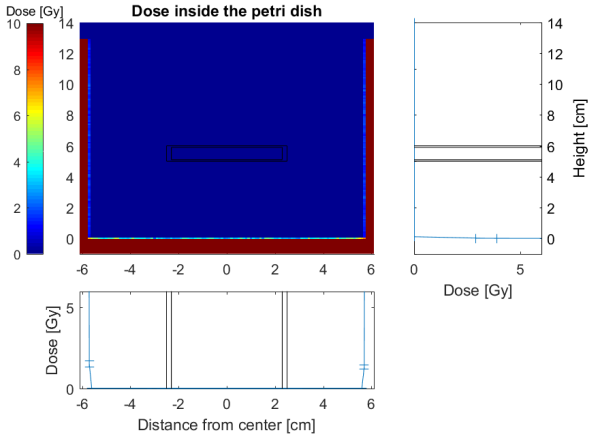

(c) Air

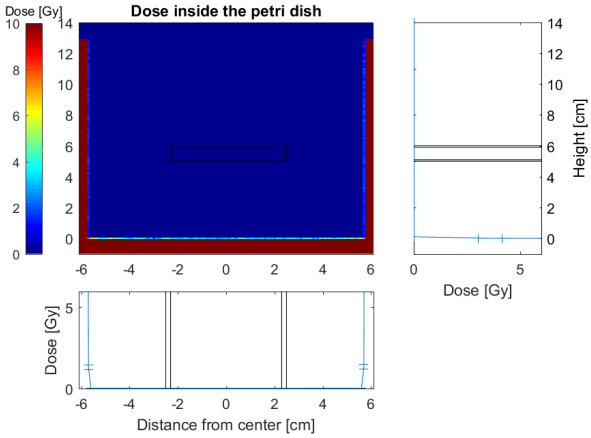

(d) Air 2

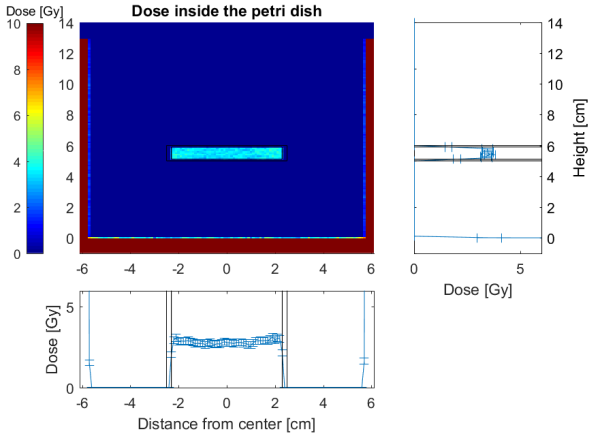

(e) Agar

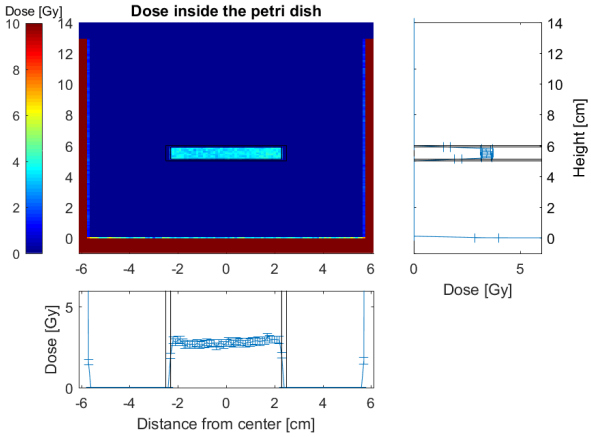

(f) Agar 2

Figure 5.1: xz section of the gc200 including sample. It shows a large field of view with half of the pencils shown on the right and the left and the petri dish in the middle. The black lines show the boundary of the petri dish and an averaged top view and side view are shown.

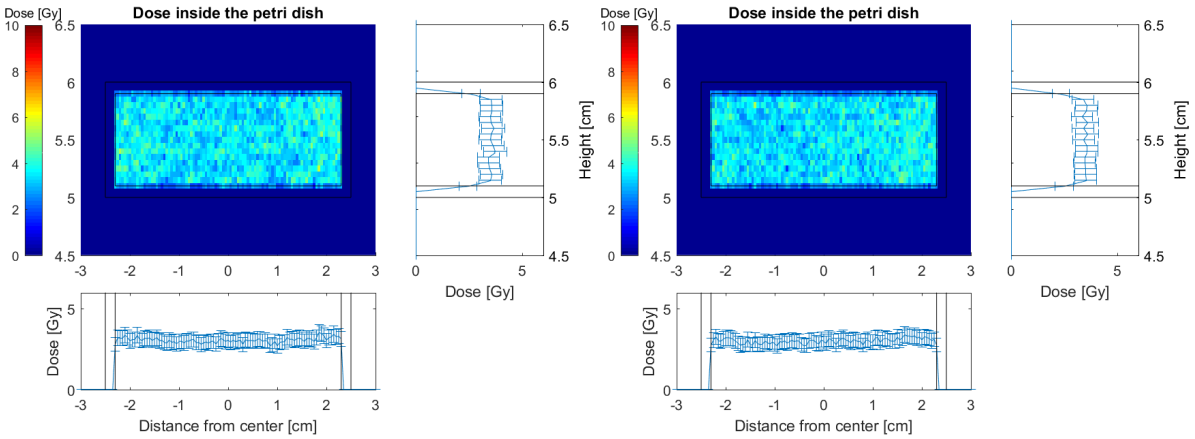

(a) Water

(b) Water 2

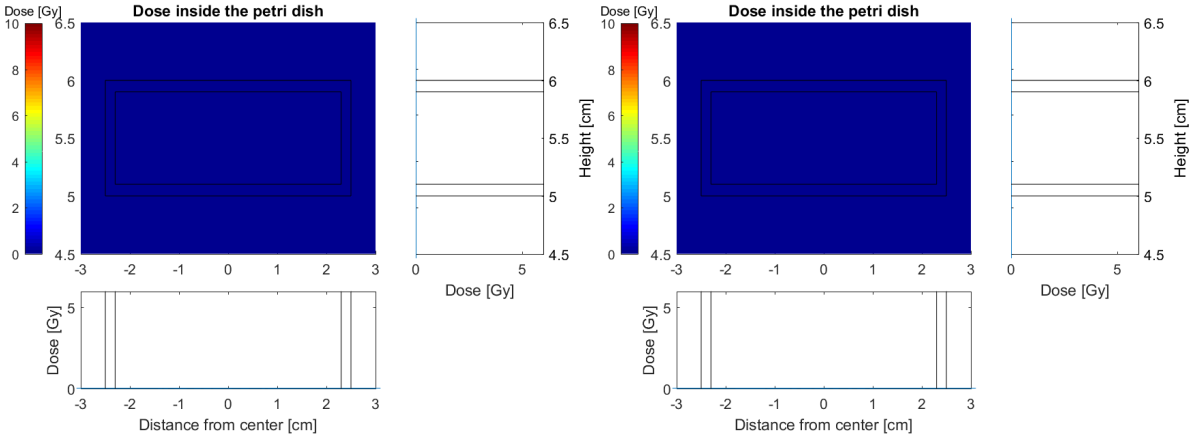

(c) Air

(d) Air 2

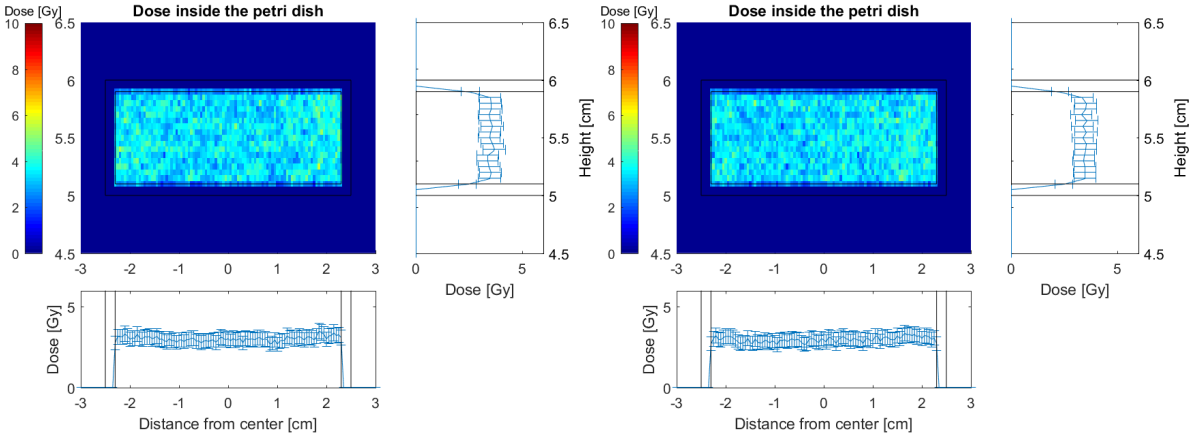

(e) Agar

(f) Agar 2

Figure 5.2: xz section of the gc200. A zoom in on the sample. The black lines show the boundary of the petri dish and an averaged top view and side view are shown.

In figure 5.1 the dose deposition in photon mode is shown. The dose is high inside the pencils. The petri dish is outlined in black, both the outline of the plastic and the outline of the contents is shown. For the petri dish filled with water and with 2% agarose the dose is about 4 Gray, which is consistent with table 5.1. The dose deposition in photon mode in air is close to zero, as no coupled transport is calculated for these figures. Figure 5.2 is a zoom of figure 5.1 and the results are the same.

5.2. Radiobiology

The embryos are irradiated in the ^{60}Co irradiator and the either the matching is measured or the embryos are fixated and used for immunohistochemistry. The results of the hatching are fitted and the fitting parameters are shown as well as the plots. The results of the staining procedures are processed and the results are displayed. A selection of images is shown below, the imageJ code is shown in appendix E.

5.2.1. Hatching

To investigate the influence of the stage of development on the hatching rate. The embryos were irradiated at 24 hpf, at 27 hpf and 30 hpf. For irradiation they were transported to the RID in the cardboard styrofoam box construction and a control group was also taken. As the irradiation takes place in the dark the control group was kept in the dark for the entire irradiation time. The embryos received a total dose of five Gray. The results are plotted in figure 5.3. For clarity the controls are not shown. The controls are shown in appendix D.

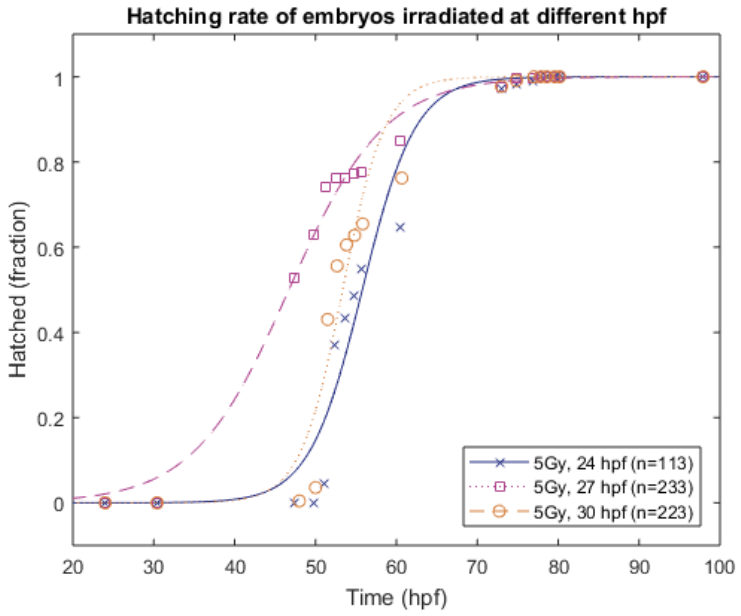

Figure 5.3: Hatching rate of embryos irradiated at a different hpf. The total dose is 5 Gy and the dose-rate is 0.015 Gy/s.

Table 5.2: Mean hatching time (HT50) for different hpf

Dose	HT_{50}	**Slope**
0 Gy, 24 hpf	54.62 ± 0.50	0.33 ± 0.06
5 Gy, 24 hpf	55.78 ± 0.58	0.30 ± 0.06
0 Gy, 27 hpf	51.09 ± 0.22	0.27 ± 0.02
5 Gy, 27 hpf	46.71 ± 0.54	0.17 ± 0.02
0 Gy, 30 hpf	51.96 ± 0.22	0.78 ± 0.13
5 Gy, 30 hpf	53.36 ± 0.41	0.38 ± 0.07

Figure 5.3 shows the hatching curves for different irradiation times for the embryos, they are irradiated at 24, 27 and 30 hpf. The embryos irradiated at 24 and 30 hpf have a comparable mean hatching time, whereas the embryos that have been irradiated at 27 hpf have an earlier mean hatching time and a more gradual slope.

To investigate total dose effects multiple total doses were researched. The irradiation time of 10 Gy was double the time of 5 Gy and the irradiation time of 20 Gy was double the time of 10 Gy. After irradiation the hatching was monitored. The results are shown in figure 5.4.

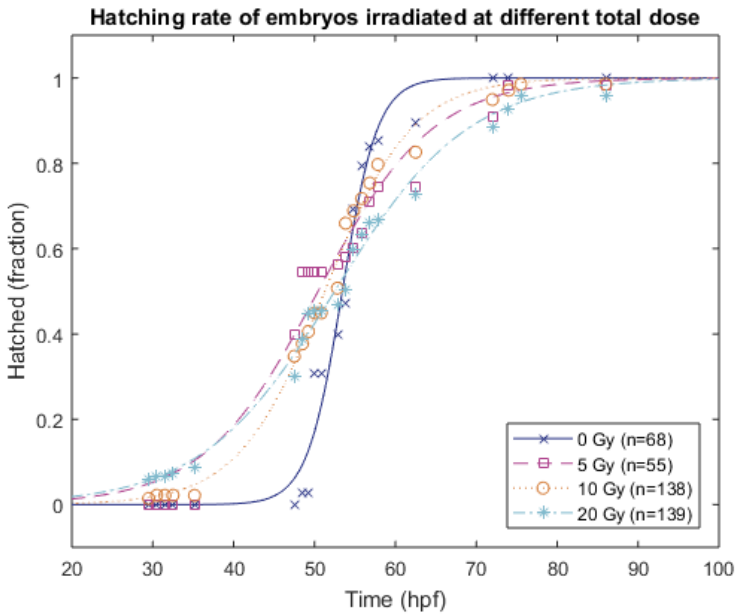

Figure 5.4: Hatching rate of embryos that received 5,10 and 20 Gy with a dose-rate of 0.015 Gy/s

Table 5.3: Mean hatching time (HT50) for different total doses

Dose	HT_{50}	**Slope**
0 Gy	53.44 ± 0.23	0.46 ± 0.04
5 Gy	50.43 ± 0.58	0.14 ± 0.02
10 Gy	51.26 ± 0.21	0.19 ± 0.01
20 Gy	52.49 ± 0.29	0.12 ± 0.01

Figure 5.4 shows that the slopes of the irradiated embryos are more gradual than the slope of the non irradiated embryos, this can also be observed in table 5.3. Irradiation seems to increase the variance of the hatching.

To investigate dose-rate effects. The embryos were irradiated with 5 Gy at a dose-rate of 0.0015 Gy/s and 0.0008 Gy/s. After irradiation the hatching was monitored. The results are shown in figure 5.6 and 5.5.

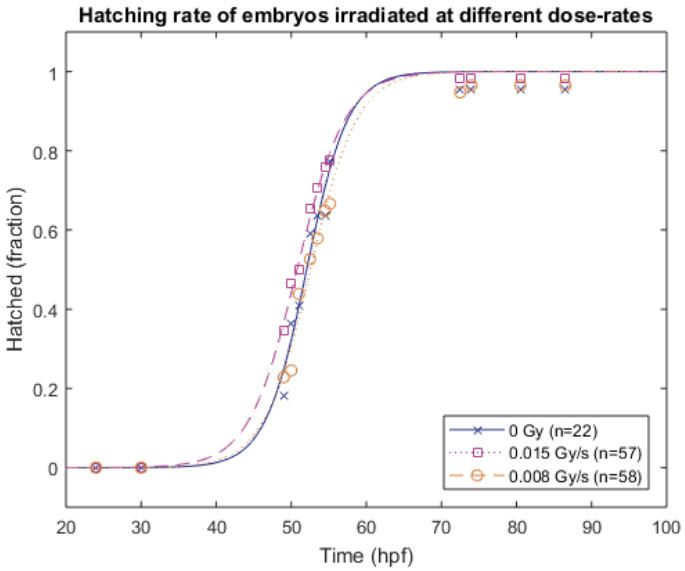

Figure 5.5: Hatching rate of embryos that received 10 Gy with a dose-rate of 0.015 Gy/s. Experiment 1

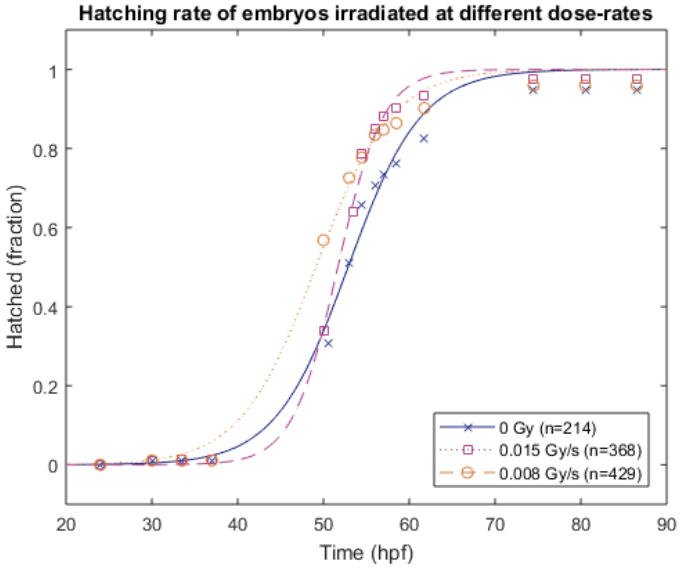

Figure 5.6: Hatching rate of embryos that received 10 Gy with a dose-rate of 0.015 Gy/s. Experiment 2

Table 5.4: Mean hatching time (HT50) for different dose-rates

	First experiment		Second experiment	
Dose	HT_{50}	**Slope**	HT_{50}	**Slope**
0 Gy	52.87 ± 0.39	0.23 ± 0.03	52.05 ± 0.23	0.36 ± 0.04
10 Gy, 0.008 Gy/s	51.68 ± 0.20	0.38 ± 0.03	50.77 ± 0.12	0.31 ± 0.02
10 Gy, 0.015 Gy/	49.12 ± 0.45	0.23 ± 0.02	52.55 ± 0.21	0.32 ± 0.03

In table 5.5 the combined results of both dose-rate experiments are shown. The results are combined using a weighted mean. The mean hatching time is a little earlier for the irradiated samples and the slope more gradual, as has been consistent in the other experiments. No clear difference in the two dose-rate groups could be observed.

Table 5.5: Mean hatching time (HT50) for different total doses combined for both dose-rate experiments

Dose	HT_{50} **combined**	**Slope combined**
0 Gy	52.79 ± 0.38	0.24 ± 0.03
10 Gy, 0.008 Gy/s	51.57 ± 0.19	0.37 ± 0.31
10 Gy, 0.015 Gy/	49.58 ± 0.43	0.43 ± 0.20

5.2.2. IHC measurements for apoptosis

The staining of caspase-3 was achieved using Anti-Caspase-3 antibody obtained from abcam (ab13847), with a secondary antibody is a donkey Anti-Rabbit IgG H&L (Alexa Fluor® 647). The concentrations are respectively 1:500 and 1:400 mM. The DAPI staining was achieved using a 1:5000 solution.

The Thapsigargon staining turned out not to be effective so it is therefore not included in the imaging.

After imaging the stacks are processed using a treshold, to filter out the background and a bitwise AND operation to compare the nucleus stain and the anti-caspase-3 stain. The results are shown in figure 5.7a and 5.7b.

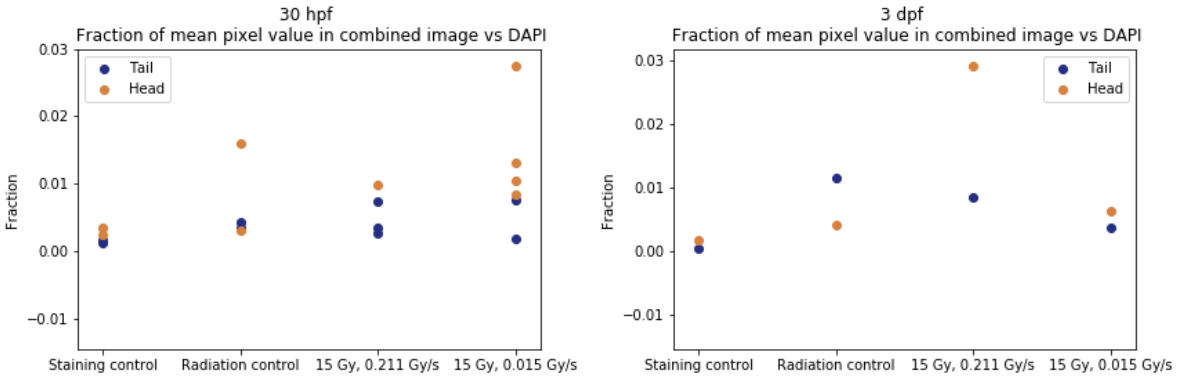

(a) 30 hours post fertilization

(b) 3 days post fertilization

Figure 5.7: Anti-Caspase-3 staining results

5.2.3. TUNEL staining for DNA breaks

The TUNEL staining was achieved using the TUNEL staining kit was obtained from abcam (ab66108) and the dilutions were according to the abcam protocol. The DAPI staining was achieved using a 1:5000 solution.

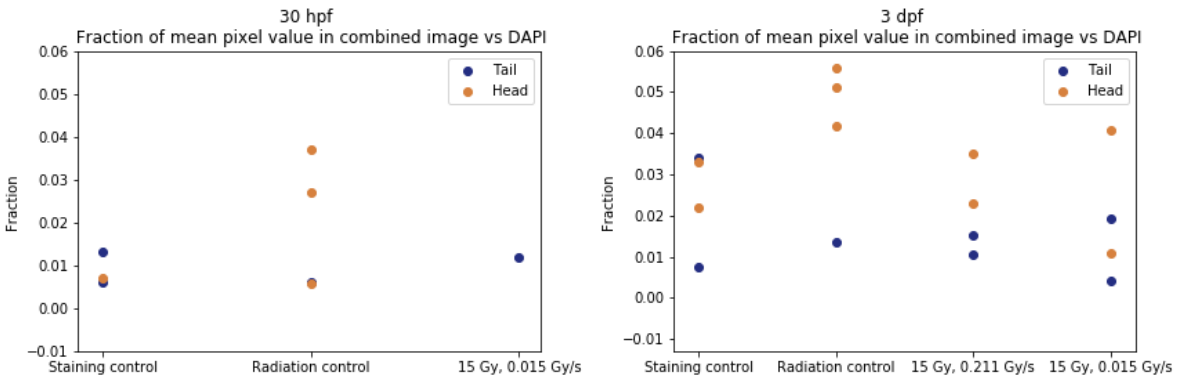

(a) 30 hours post fertilization

(b) 3 days post fertilization

Figure 5.8: TUNEL staining results

5.2.4. Data processing of confocal imaging results

The next two pages show images made with the confocal microscope. Figure 5.9 and 5.10 shows maximum projections of the DAPI and the anti-caspase-3 staining and the combination of both. Figure 5.11 and 5.12 shows the result of the processing.

In the figures the DAPI staining and the anti-caspase-3 staining can be observed. Figure 5.9 and 5.10 are used to observe colocalization of the DAPI (cell nuclei) and the staining. As can be observed the DAPI and the staining are colocalized indicating that the staining is effective. Both the DAPI and the staining images are thresholded and a bit-wise comparision is executed. After applying a "Red Hot" color map the resulting image can be observed in figure 5.11 and 5.12. The pixel value with a high intensity means that there is a stained nuclei and a anti-caspase-3 staining. Colocalization of both signals indicates apoptosis.

In the figures 5.13 and 5.14 both the DAPI and the TUNEL staining can be observed as well as the colocalization. The colocalization seems very good in 5.14 and as there is no clear staining visible in figure 5.13 it can not be said from figure 5.13. However it is good that there is no clear staining visible as this embryo is part of the control to the staining method group. However from both of these figures a lot of autofluorescence can be observed, especially in the green channel. In the images after processing, figure 5.15 and 5.16, which has been executed the same as IHC, can a clear difference between irradiated samples and non irradiated samples be observed. The arrow points to the brain area where a lot more signal is compared to the control, this means that the area is likely damaged by radiation. This phenomenon can be observed in more samples. However there is not yet enough data to quantify this effect.

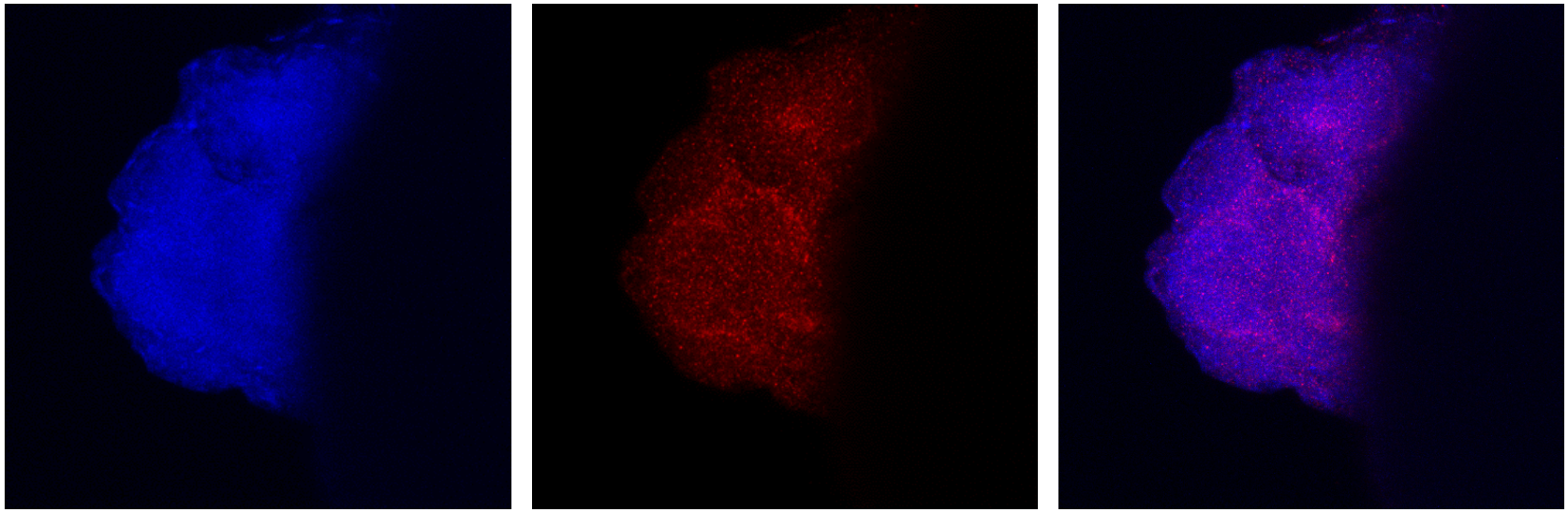

(a) DAPI staining (b) Anti-caspase-3 staining (c) Colocalization

Figure 5.9: Maximum projections of confocal imaging results. It shows a 30 hpf embryo, that has been irradiated with 0.0015 Gy/s at 24 hpf for a total dose of 15 Gy.

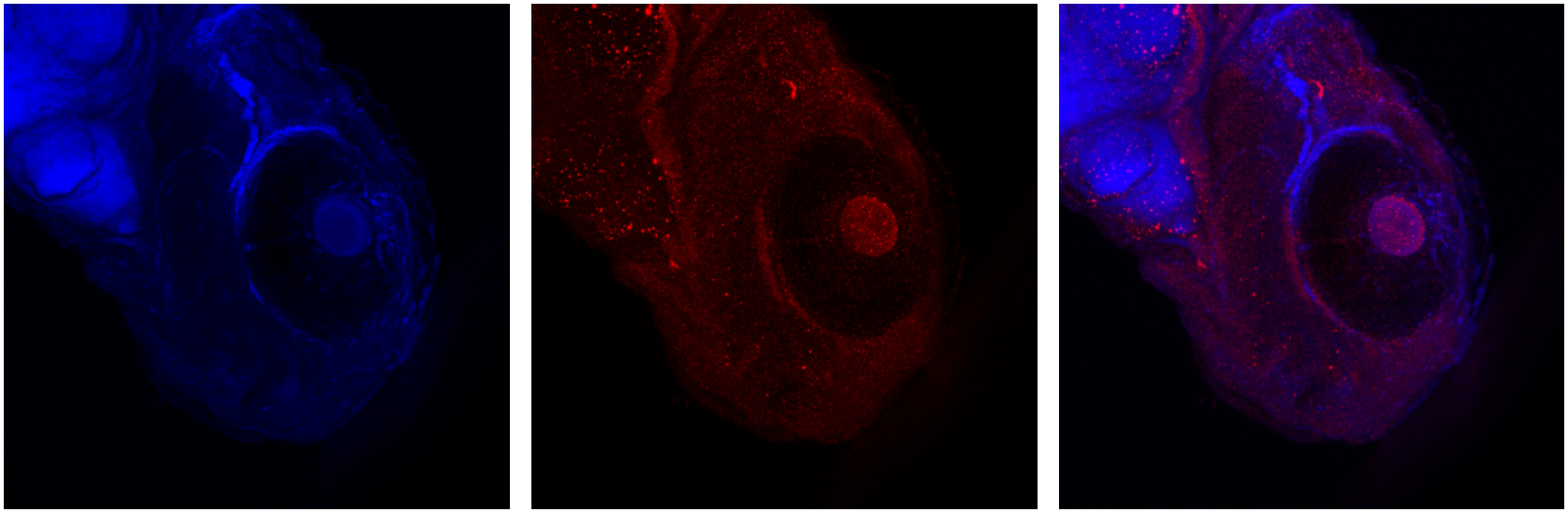

(a) DAPI staining (b) Anti-caspase-3 staining (c) Colocalization

Figure 5.10: Maximum projections of confocal imaging results. It shows a 3 dpf embryo, that has not been irradiated.

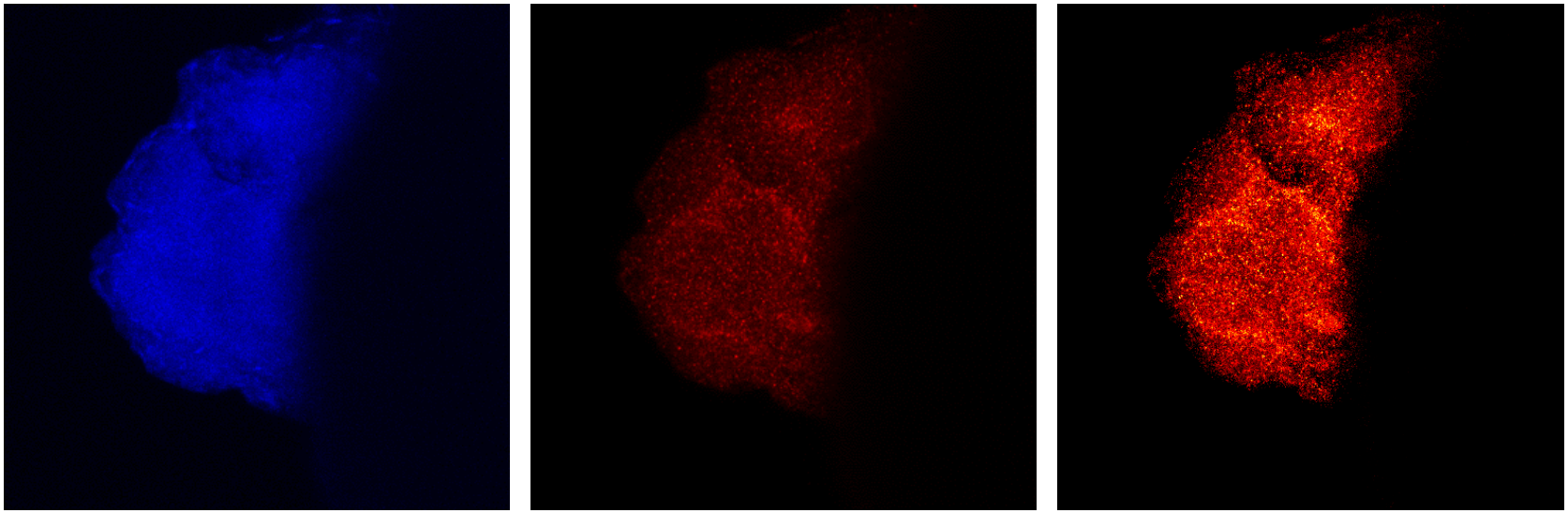

(a) DAPI staining (b) Anti-caspase-3 staining (c) Post processing

Figure 5.11: Maximum projections of confocal imaging results. It shows a 30 hpf embryo, that has been irradiated with 0.0015 Gy/s at 24 hpf for a total dose of 15 Gy.

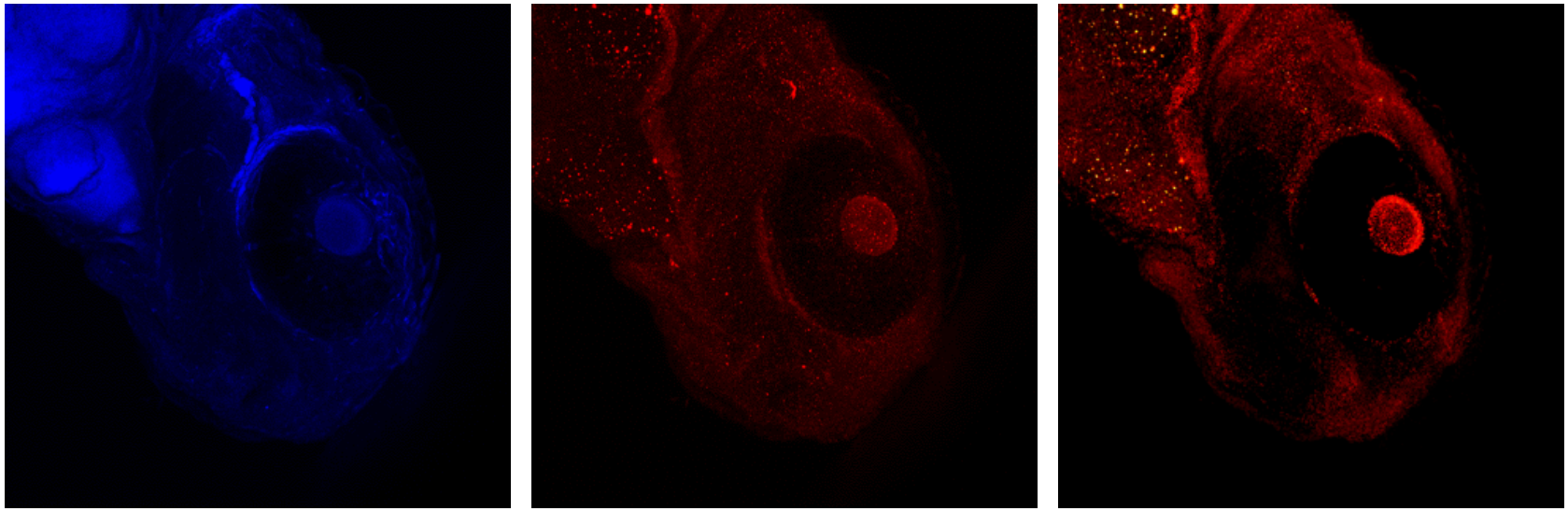

(a) DAPI staining (b) Anti-caspase-3 staining (c) Post processing

Figure 5.12: Maximum projections of confocal imaging results. It shows a 3 dpf embryo, that has not been irradiated.

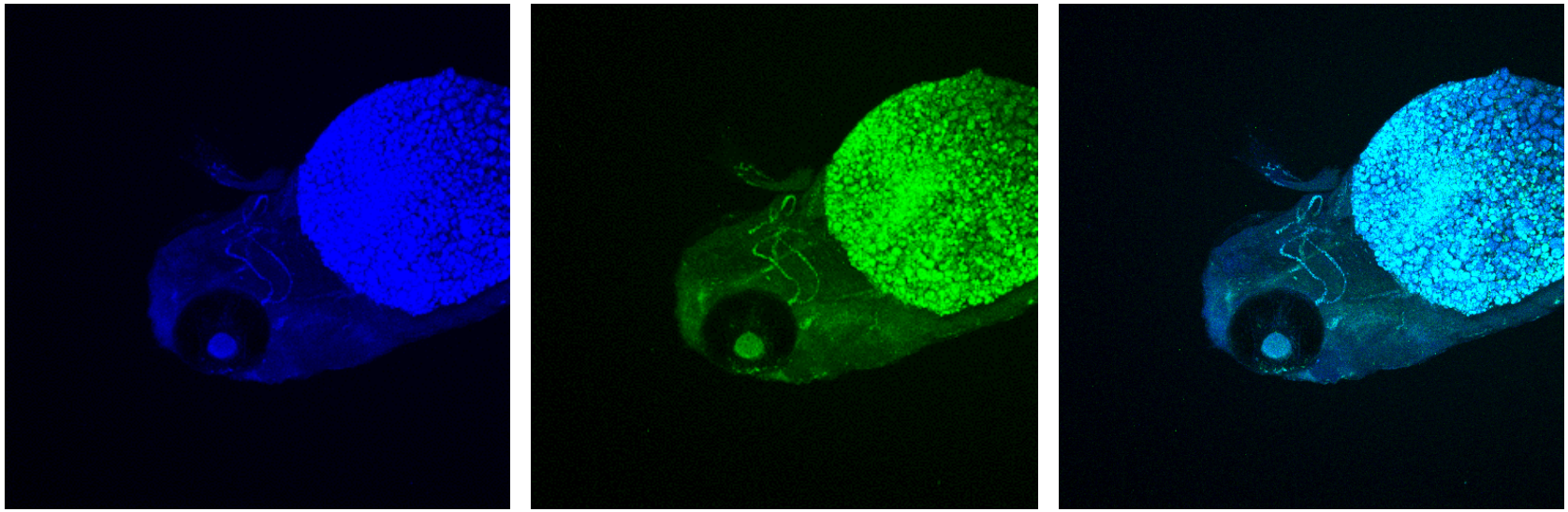

(a) DAPI staining (b) TUNEL staining (c) Colocalization

Figure 5.13: Maximum projections of confocal imaging results. It shows a 3 dpf embryo, that has received no irradiation and no TdT enzyme. The staining method is TUNEL staining.

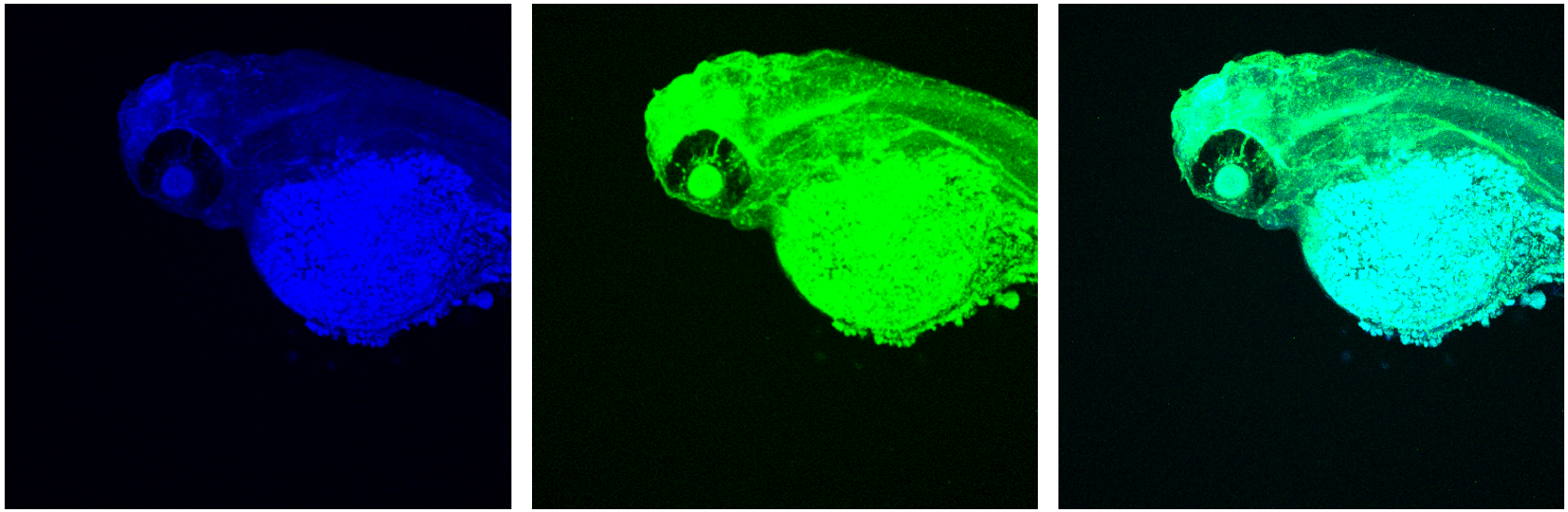

(a) DAPI staining (b) TUNEL staining (c) Colocalization

Figure 5.14: Maximum projections of confocal imaging results. It shows a 3 dpf embryo, that has been irradiated with 0.211 Gy/s at 24 hpf for a total dose of 15 Gy.

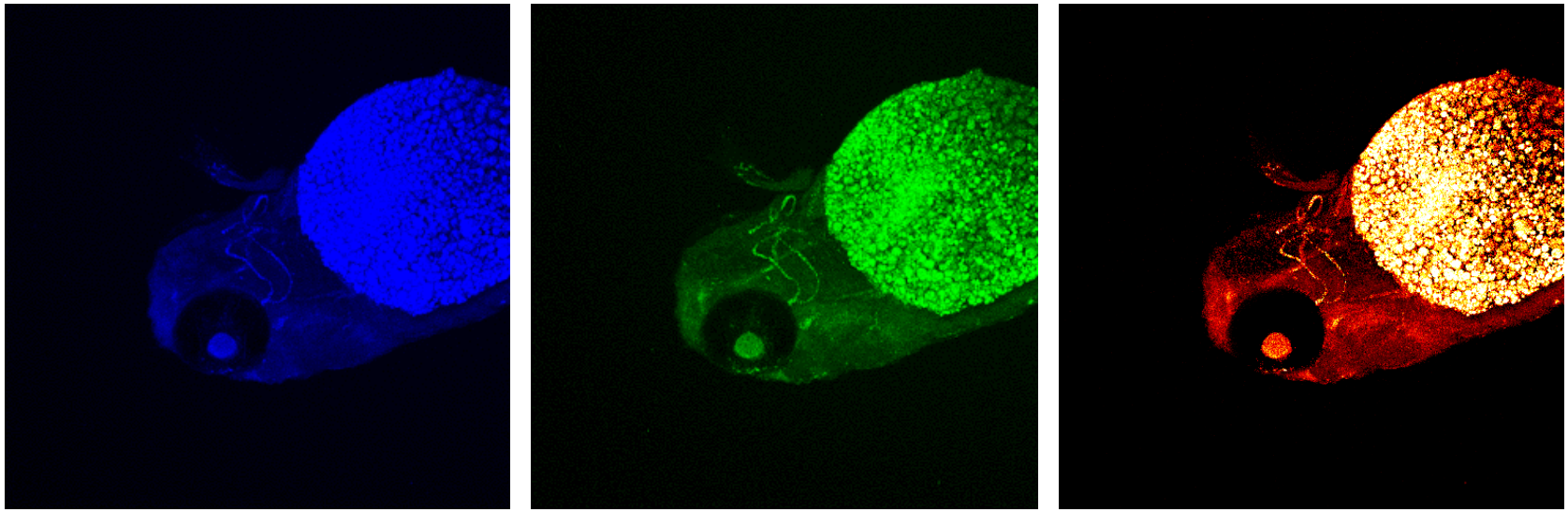

(a) DAPI staining (b) TUNEL staining (c) Post processing

Figure 5.15: Maximum projections of confocal imaging results. It shows a 3 dpf embryo, that has received no irradiation and no TdT enzyme. The staining method is TUNEL staining.

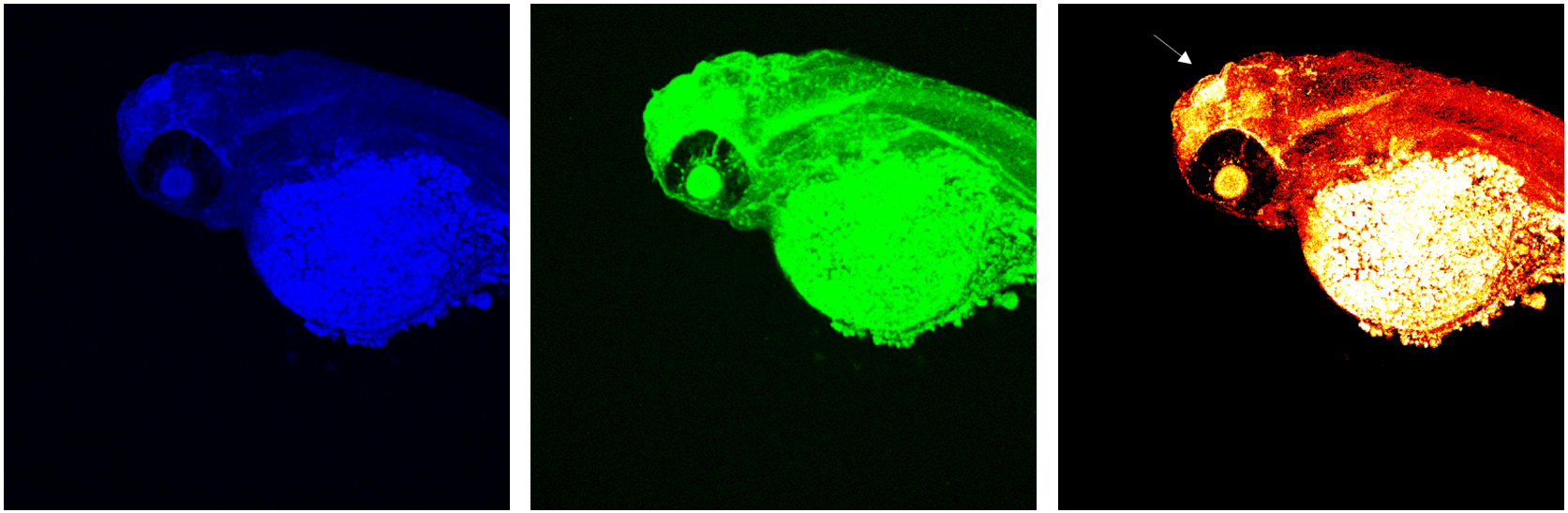

(a) DAPI staining (b) TUNEL staining (c) Post processing

Figure 5.16: Maximum projections of confocal imaging results. It shows a 3 dpf embryo, that has been irradiated with 0.211 Gy/s at 24 hpf for a total dose of 15 Gy.

6

Discussion and conclusion

Monte Carlo dose calculations with MCNP

The dose-rate in Gy/s as a result from the simulation in air is $1,98 \cdot 10^{-2}$ Gy/s, while the dose-rate measured by the quality assurance measurements is $1,52 \cdot 10^{-2}$ Gy/s. The outcome of the simulations and the experimental quality assurance measurements is expected to have a similar result. A possible explanation of the difference could be the circumstances surrounding the quality assurance measurement. The dose-rate at the quality assurance measurement is measured in air without any samples or materials in the sample chamber and the measurement position is likely to be at the bottom of the sample chamber, as it is easier to place items there. The dose at the bottom is 70% of the dose at the middle of the chamber, see figure 4.3b. The middle of the sample chamber is at 6.95 cm, the simulation is evaluated at 7.5 cm from the bottom of the sample chamber. This is in accordance with the experimental procedure. At this position the dose is 95% according to figure 4.3b [55]. This difference could explain the difference in dose-rate. The dose at 7.5 cm height is $(0.95/0.7) * 100\% = 135\%$ of the dose at the bottom. The expected dose at 7.5 cm from the quality assurance measurements would be $1.52 \cdot 10^{-2} * 1.35 = 2,06 \cdot 10^{-2}$ Gy/s. This is consistent with the simulation result in air.

The simulated dose-rate in water and agar is 37% lower than in air. The simulated dose-rate in water and agar is 17% lower than the quality assurance measurements dose. This means that the embryos receive a lower dose than expected. The most probable explanation for the dose difference is that the petri dish is 1 cm thick. The buildup in water is about 1 cm so therefore the dose is lower than the expected dose.

The reason these simulations are important is because embryos are small and it is important to ensure that they receive the intended dose. The dose should be the same regardless of the position of the embryos in the petri dish. As can be expected the photon FMESH shows that the photon dose is constant throughout the dish. However the biggest uncertainty results from the electron behaviour. Unfortunately the electron FMESH verification did not provide reliable results. Therefor the electron FMESH are not included. For now this question remains unanswered.

Hatching

The hatching experiments show that irradiation with 0.015 Gy/s do and 0.211 Gy/s do not change the mean hatching time. However irradiation does influence the variance on hatching. The irradiated embryos have a greater variance in when they hatch compared to the unirriated embryos. Since this experiment did not find a clear difference between the two dose-rates in mean hatching time, a more sensitive biomarker is needed. Biomarkers for apoptosis and DNA damage are known biomarkers for radiation damage and are more sensitive and specific.

Staining

The biological effects are observed on a sub-cellular scale. Two time points were taken, 30 hpf and 3 dpf to observe cell damage and possible cell repair. The cell damage was assessed using TUNEL staining to indicate DNA breaks and caspase-3 IHC to asses cell death.

The staining control group has a low value compared to the samples that have been stained, this indicates specific binding of the primairy antibody. Unfortunally not enough samples were measured to obtain accurate statistics to quantify dose-rate effects. When observing the confocal imaging results the irradiated

samples contain more damaged cells than the non irradiated samples. However a lot more data is needed for a scientifically based conclude if dose-rate effects apoptosis. The difference will most likely be more defined by a bigger increase in the dose-rate. Even going up to FLASH dose-rates will provide more relevant information as to the extent of the biological impact of dose-rate on apoptosis.

A positive control will give a better idea about the extent of the damage induced by radiation. A experiment with working Thapsigargon will help to asses the damage in the cells.

For the TUNEL staining the staining control shows higher values than the IHC. This may be caused by unspecific staining. However looking at the images it seems to result from autofluorescence from the yolk. That also explains why the values in the head are higher than the values in the tail, as the head contains much more autofluorescence.

Thapsigargon does not cause DNA breaks, therefore it cannot be used as a positive control for the TUNEL staining. Another chemical should be used to serve as positive control. Another possibility is to use 250 kV xrays as a control for all types of staining. This way the control is similar across all methods.

Next steps

This thesis provides the reader a lot of information on the dose deposited in just a small amount of water. As the embryos are small it is important to understand the dose that they receive for accurate and reproducible experimental results. This thesis also provides the reader with the background and understanding in order to conduct research into the biological effects of different dose-rate or possibly even the "FLASH effect". This information along with the staining protocols developed in this research can be used to do more extensive research on dose-rate effects in the future. Especially the ability to stain whole-mount zebrafish instead of sections can provide a lot of spatial information. These whole-mount protocols enable the researcher to find specific area's inside the zebrafish that are more affected by irradiation or area's that are more radioresistant.

Future research

This research explores different biomarkers for measuring dose-rate effects. It is limited by the dose-rates available at the time of the research. Thus in future research FLASH dose-rates need to be achieved for a good assessment of the biological effects of high dose-rate radiation. Using all

DNA damage is the main contributor to apoptosis, however the working mechanisms of a cell are more extensive. High dose-rate radiation could influence ROS prevalence, energy production or protein formation. More biomarkers can be researched to gain a fuller picture of the biological effects of high dose-rate radiation.

It is also important to understand the difference in how a tumor cell responds to radiation compared to healthy cells in vivo. Besides investigating how tumor cells responds to one fraction, it is also important to understand how tumor and healthy cells respond to multiple fractions with different time in between fractions.

In conclusion, sub-cellular DNA damage and apoptotic biomarkers provide information about the reaction of tissues to radiation. In order to fully understand dose-rate effects more data on higher dose-rates, a greater variety of biomarkers, tumorous tissue and a greater variety of radiation parameters is needed to obtain a better understanding of FLASH effects on a biological level.

Bibliography

[1] Abcam. TUNEL Assay Kit (ab66108) , N.D. URL https://www.abcam.com/tunel-assay-kit-fitc-ab66108.html. Accessed on 2019-11-28.

[2] American Cancer Society. External Beam Radiation Therapy, 2017. URL https://www.cancer.org/treatment/treatments-and-side-effects/treatment-types/radiation/external-beam-radiation-therapy.html. Accessed on 2019-10-08.

[3] J. Armstrong, F.B. Brown, J.S. Bull, L. Casswell, L.J. Cox, D. Dixon, R.A. Forster, John T. Goorley, H.G. Hughes, J. Favorite, R. Martz, S.G. Mashnik, M.E. Rising, C. Solomon, A. Sood, J.E. Sweezy, C.J. Werner, A. Zukaitis, C. Anderson, J.S. Elson, J.W. Durkee, R.C. Johns, G.W. McKinney, G.E. McMath, J.S. Hendricks, D.B. Pelowitz, R.E. Prael, T.E. Booth, M.R. James, M.L. Fensin, T.A. Wilcox, and B.C. Kiedrowski. *Monte Carlo N–Particle® Transport Code System Version 6.2*. Los Alamos National Laboratory, Los Alamos, New Mexico, OAK RIDGE, 2017.

[4] S. Auer, V. Hable, C. Greubel, G.A. Drexler, T.E. Schmid, C. Belka, G. Dollinger, and A.A. Friedl. Survival of tumor cells after proton irradiation with ultra-high dose rates. *Radiation Oncology*, 6(1):139, 2011. ISSN 1748-717X. doi: 10.1186/1748-717X-6-139.

[5] J. Bergonié and L. Tribondeau. Interprétation de quelques résultats de la Radiothérapie et essai de fixation d'une technique rationnelle. *Comptes Rendus Des Seances De lAcadémie Des Sciences*, 143:983–985, 1906. ISSN 00337587. doi: 10.2307/3570812.

[6] E. Beyreuther, L. Karsch, L. Laschinsky, E. Lessmann, D. Naumburger, M. Oppelt, C. Richter, M. Schurer, J. Woithe, and J. Pawelke. Radiobiological response to ultra-short pulsed megavoltage electron beams of ultra-high pulse dose rate. *International journal of radiation biology*, 91(8):643–652, aug 2015. ISSN 1362-3095 (Electronic). doi: 10.3109/09553002.2015.1043755.

[7] E. Beyreuther, M. Brand, S. Hans, K. Hideghéty, L. Karsch, E. Leßmann, M. Schürer, E.R. Szabó, and J. Pawelke. Feasibility of proton FLASH effect tested by zebrafish embryo irradiation. *Radiotherapy and Oncology*, 139:46–50, oct 2019. ISSN 18790887. doi: 10.1016/j.radonc.2019.06.024.

[8] K. Boland, L. Flanagan, and J.H.M. Prehn. Paracrine control of tissue regeneration and cell proliferation by Caspase-3. *Cell Death and Disease*, 4(7), jul 2013. ISSN 20414889. doi: 10.1038/cddis.2013.250.

[9] A.J.J. Bos, F.S. Draaisma, and W.J.C. Okx. *Inleidning tot de stralingshygiëne*. Sdu Uitgevers, Den Haag, 2007. ISBN 9789012119054.

[10] J. Bourhis, P. Montay-Gruel, P. Gonçalves Jorge, C. Bailat, B. Petit, J. Ollivier, W. Jeanneret-Sozzi, M. Ozsahin, F. Bochud, R. Moeckli, J.F. Germond, and M.C. Vozenin. Clinical translation of FLASH radiotherapy: Why and how?, oct 2019. ISSN 18790887.

[11] A. Collins, M. Dušinská, M. Franklin, M. Somorovská, S. Petrovská, H.and Duthie, L. Fillion, M. Panayiotidis, K. Rašlová, and N. Vaughan. Comet assay in human biomonitoring studies: Reliability, validation, and applications. *Environmental and Molecular Mutagenesis*, 30(2):139–146, jan 1997. ISSN 08936692. doi: 10.3389/conf.fgene.2015.01.00019.

[12] Andrew R. Collins. The comet assay for dna damage and repair. *Molecular Biotechnology*, 26(3):249, Mar 2004. ISSN 1559-0305. doi: 10.1385/MB:26:3:249.

[13] Genome Reference Consortium. Zebrafish Genome Overview, 2017. URL https://www.ncbi.nlm.nih.gov/grc/zebrafish.

[14] R. Dahm. The Zebrafish Exposed: "See-through" mutants may hold the key to unraveling the mysteries of embryonic development, 2006. URL https://www.jstor.org/stable/27858837.

[15] A. Devaux, P. Flammarion, V. Bernardon, J. Garric, and G. Monod. Monitoring of the chemical pollution of the river Rhône through measurement of DNA damage and cytochrome P4501a induction in chub (Leuciscus cephalus). *Marine Environmental Research*, 46(1-5):257–262, jul 1998. ISSN 0141-1136. doi: 10.1016/S0141-1136(97)00105-0.

[16] N.I. Dmitrieva and M.B. Burg. Osmotic Stress and DNA Damage. *Methods in Enzymology*, 428:241–252, jan 2007. ISSN 0076-6879. doi: 10.1016/S0076-6879(07)28013-9.

[17] M. Ekker and M.A. Akimenko. Genetic tools. In Steve F Perry, Marc Ekker, Anthony P Farrell, and Colin J B T Fish Physiology Brauner, editors, *Zebrafish*, volume 29, pages 1–23. Academic Press, 2010. ISBN 1546-5098. doi: https://doi.org/10.1016/S1546-5098(10)02901-8.

[18] E.R. Epp, H. Weiss, B. Djordjevic, and A. Santomasso. The Radiosensitivity of Cultured Mammalian Cells Exposed to Single High Intensity Pulses of Electrons in Various Concentrations of Oxygen. *Radiation Research*, 52(2):324, nov 1972. ISSN 00337587. doi: 10.2307/3573572.

[19] V. Favaudon, L. Caplier, V. Monceau, F. Pouzoulet, M. Sayarath, C. Fouillade, M.F. Poupon, I. Brito, P. Hupe, J. Bourhis, J. Hall, J.J. Fontaine, and M.C. Vozenin. Ultrahigh dose-rate FLASH irradiation increases the differential response between normal and tumor tissue in mice. *Science translational medicine*, 6(245):245ra93, jul 2014. ISSN 1946-6242 (Electronic). doi: 10.1126/scitranslmed.3008973.

[20] V Favaudon, C Fouillade, and M.C. Vozenin. [Ultrahigh dose-rate, "flash" irradiation minimizes the side-effects of radiotherapy]. *Cancer radiotherapie*, 19(6-7):526–531, oct 2015. ISSN 1769-6658 (Electronic). doi: 10.1016/j.canrad.2015.04.006.

[21] D. Feilzer. *Gd-PSMA Neutro Capture Therapy: Acomputational feasibility and method development study*. PhD thesis, Tu Delft, 2018.

[22] B. Ford and R. Shannon. Microscope, nov 2019. URL `https://www.britannica.com/technology/microscope/Confocal-microscopes`.

[23] B. Gagnaire, I. Cavalie, V. Camilleri, and C. Adam-Guillermin. Effects of Depleted Uranium on Oxidative Stress, Detoxification, and Defence Parameters of Zebrafish Danio rerio. *Archives of Environmental Contamination and Toxicology*, 64(1), 2013. doi: 10.1007/s00244-012-9814-z.

[24] B. Gagnaire, I. Cavalie, S. Pereira, M. Floriani, N. Dubourg, V. Camilleri, and C. Adam-Guillermin. External gamma irradiation-induced effects in early-life stages of zebrafish, Danio rerio. *Aquatic toxicology*, 169:69–78, dec 2015. ISSN 1879-1514 (Electronic). doi: 10.1016/j.aquatox.2015.10.005.

[25] L. Gerweck and H. Paganetti. Radiobiology of charged particles. In *Proton and Charged Particle Radiotherapy*, pages 8–18. Lippincott Williams & Wilkins, Philadelphia PA, 2008.

[26] W. Gorczyca, S. Bruno, R.J. Darzynkiewicz, J.P. Gong, and Z. Darzynkiewicz. DNA strand breaks occuring during apoptosis - their early insitu detection by the terminal deoxynucleotidyl transverase and nick translation assays and prevention by serine protease inhibitors. *International Journal of Oncology*, 1(6): 639–648, nov 1992. ISSN 1019-6439. doi: 10.3892/ijo.1.6.639.

[27] J.V. Guttag. *Introduction to computation and programming using python*. MIT Press, Massachusetts, second edition, 2016.

[28] E.J. Hall. *Radiobiology for the Radiologist*. Lippincottt Williams & Wilkins, 2010.

[29] J. Hao, A. Godley, J.D. Shoemake, Z. Han, A. Magnelli, and J.S. Yu. The effects of extra high dose rate irradiation on glioma stem-like cells. *PloS one*, 13:8, 2018. ISSN 1932-6203 (Electronic). doi: 10.1371/journal.pone.0202533.

[30] A.C. Hermann, P.J. Millard, S.L. Blake, and C.H. Kim. Development of a respiratory burst assay using zebrafish kidneys and embryos. *Journal of Immunological Methods*, 292(1-2):119–129, sep 2004. ISSN 0022-1759. doi: 10.1016/J.JIM.2004.06.016.

[31] S. Hurem, L.M. Martin, D.A. Brede, E. Skjerve, R. Nourizadeh-Lillabadi, O.C. Lind, T. Christensen, V. Berg, H.C. Teien, B. Salbu, D.H. Oughton, P. Alestrom, and J.L. Lyche. Dose-dependent effects of gamma radiation on the early zebrafish development and gene expression. *PloS one*, 12:6, 2017. ISSN 1932-6203 (Electronic). doi: 10.1371/journal.pone.0179259.

[32] IAEA. Effects of Ionizing Radiation on Plants and Animals at Levels Implied by Current Radiation Protection Standards. Technical report, International Atomic Energy Agency, Vienna, 1992. URL `https://www.iaea.org/publications/1436/effects-of-ionizing-radiation-on-plants-and-animals-at-levels-implied\-by-current-radiation-protection-standards`.

[33] IAEA. Gamma Irradiators For Radiation Proscessing. Technical report, International Atomic Energy Agency, 2005.

[34] IAEA. Livechart - Table of Nuclides - Nuclear structure and decay data, N.D. URL `https://www-nds.iaea.org/relnsd/vcharthtml/VChartHTML.html`. Accessed on 2019-10-21.

[35] G.H. Jang, J.H. Ha, T.L. Huh, and Y.M. Lee. Effect of proton beam on blood vessel formation in early developing zebrafish (Danio rerio) embryos. *Archives of Pharmacal Research*, 31(6):779, 2008. ISSN 1976-3786. doi: 10.1007/s12272-001-1226-1.

[36] F.M. Khan. *The physics of radiation therapy*. Lippincott Williams & Wilkins, 2014. ISBN 9781451182453.

[37] E. H. KIM. Radiation therapy for cancer. *Taehan Ŭihak Hyŏphoe chi. The Journal of the Korean Medical Association*, 6:142–146, feb 1963. ISSN 00234028. doi: 10.1596/978-1-4648-0349-9_ch14.

[38] C.B. Kimmel, W.W. Ballard, S.R. Kimmel, B. Ullmann, and T.F. Schilling. Stages of embryonic development of the zebrafish. *Developmental Dynamics*, 203(3):253–310, jul 1995. ISSN 10588388. doi: 10.1002/aja.1002030302.

[39] L. Laschinsky, M. Baumann, E. Beyreuther, W. Enghardt, M. Kaluza, L. Karsch, E. Lessmann, D. Naumburger, M. Nicolai, C. Richter, R. Sauerbrey, H.P. Schlenvoigt, and J. Pawelke. Radiobiological effectiveness of laser accelerated electrons in comparison to electron beams from a conventional linear accelerator. *Journal of radiation research*, 53(3):395–403, 2012. ISSN 1349-9157 (Electronic).

[40] L Laschinsky, L Karsch, E. Lessmann, M. Oppelt, J. Pawelke, C. Richter, M. Schurer, and E. Beyreuther. Radiobiological influence of megavoltage electron pulses of ultra-high pulse dose rate on normal tissue cells. *Radiation and environmental biophysics*, 55(3):381–391, aug 2016. ISSN 1432-2099 (Electronic). doi: 10.1007/s00411-016-0652-7.

[41] I. Lohse, S. Lang, J. Hrbacek, S. Scheidegger, S. Bodis, N.S. Macedo, J. Feng, U.M. Lutolf, and K. Zaugg. Effect of high dose per pulse flattening filter-free beams on cancer cell survival. *Radiotherapy and oncology : journal of the European Society for Therapeutic Radiology and Oncology*, 101(1):226–232, oct 2011. ISSN 1879-0887 (Electronic). doi: 10.1016/j.radonc.2011.05.072.

[42] T. Matsuura, Y. Egashira, T. Nishio, Y. Matsumoto, M. Wada, S. Koike, Y. Furusawa, R. Kohno, S. Nishioka, S. Kameoka, K. Tsuchihara, M. Kawashima, and T. Ogino. Apparent absence of a proton beam dose rate effect and possible differences in RBE between Bragg peak and plateau. *Medical physics*, 37(10): 5376–5381, oct 2010. ISSN 0094-2405 (Print). doi: 10.1118/1.3490086.

[43] S.J. McMahon. The linear quadratic model: usage, interpretation and challenges Recent citations. *Physics in Medicine & Biology*, 64(1), 2018. doi: 10.1088/1361-6560/aaf26a. URL `https://doi.org/10.1088/1361-6560/aaf26a`.

[44] H.B. Michaels, E.R. Epp, C.C. Ling, and E.C. Peterson. Oxygen Sensitization of CHO Cells at Ultrahigh Dose Rates: Prelude to Oxygen Diffusion Studies. *Radiation Research*, 76(3):510, dec 1978. ISSN 00337587. doi: 10.2307/3574800.

[45] P. Montay-Gruel, K. Petersson, M. Jaccard, G. Boivin, J.F. Germond, B. Petit, R. Doenlen, V. Favaudon, F. Bochud, C. Bailat, J. Bourhis, and M.C. Vozenin. Irradiation in a flash: Unique sparing of memory in mice after whole brain irradiation with dose rates above 100 Gy/s. *Radiotherapy and Oncology*, 124(3): 365–369, sep 2017. ISSN 18790887. doi: 10.1016/j.radonc.2017.05.003.

[46] National Cancer Institute. Definition of radiotherapy, N.D. URL https://www.cancer.gov/publications/dictionaries/cancer-terms/def/radiotherapy. Accessed on 2019-10-08.

[47] P. Noury, O. Geffard, R. Tutundjian, and J. Garric. Non destructivein vivo measurement of ethoxyresorufin biotransformation by zebrafish prolarva: Development and application. *Environmental Toxicology*, 21(4):324–331, aug 2006. ISSN 1520-4081. doi: 10.1002/tox.20184. URL http://doi.wiley.com/10.1002/tox.20184.

[48] U. Oelfke and C. Scholz. 15 Dose Calculation Algorithms. Technical report, Deutsches Krebsforschungszentrum, 2006. URL http://eknygos.lsmuni.lt/springer/315/187-196.pdf.

[49] A.G. Porter and R.U. Jänicke. Emerging roles of caspase-3 in apoptosis. *Cell Death & Differentiation*, 6 (2):99–104, feb 1999. ISSN 1350-9047. doi: 10.1038/sj.cdd.4400476.

[50] K. Ray, K. Hudak, D. Citrin, and M. Stick. Biomarkers of radiation injury and response. *Biomarkers in Toxicology*, pages 673–687, jan 2014. doi: 10.1016/B978-0-12-404630-6.00039-7.

[51] D.W.O. Rogers. Fifty years of Monte Carlo simulations for medical physics. *Physics in Medicine and Biology*, 51(13):R287–R301, jul 2006. ISSN 0031-9155. doi: 10.1088/0031-9155/51/13/R17.

[52] A. Schipler and G. Iliakis. DNA double-strand-break complexity levels and their possible contributions to the probability for error-prone processing and repair pathway choice. *Nucleic Acids Research*, 41(16): 7589–7605, sep 2013. ISSN 03051048. doi: 10.1093/nar/gkt556.

[53] Fisher Scientific. BD Apoptosis Detection Kit (APO-Direct), N.D. URL https://www.fishersci.com/shop/products/bd-apoptosis-detection-kit-apo-direct-1-kit/bdb556381.

[54] H. Simmons. Zebrafish as a Model Organism, 2019. URL https://www.news-medical.net/life-sciences/Zebrafish-as-a-Model-Organism.aspx. Accessed on 2019-11-28.

[55] B.P. Smith and R.E. Lee. A Description of 60Co Gamma Irradiation Facilities in the Radiation Biology and Health Physics Branch Description des installations d irradiation gamma an 60Co de Radiobiologie et Radioprotection. Technical report, AECL, jun 1996.

[56] J.J Stegeman, J.V. Goldstone, and M.E. Hahn. 10 - Perspectives on zebrafish as a model in environmental toxicology. In S.F. Perry, M. Ekker, A.P. Farrell, and C.J.B.T Brauner, editors, *Zebrafish*, volume 29, pages 367–439. Academic Press, 2010. ISBN 1546-5098. doi: S1546-5098(10)02910-9.

[57] T.D. Sterling, H. Perry, and L. Katz. Automation of radiation treatment planning—iv. derivation of a mathematical expression for the per cent depth dose surface of cobalt 60 beams and visualisation of multiple field dose distributions. *The British Journal of Radiology*, 37(439):544–550, 1964. doi: 10.1259/0007-1285-37-439-544.

[58] B. Tucker and M. Lardelli. A Rapid Apoptosis Assay Measuring Relative Acridine Orange Fluorescence in Zebrafish Embryos. *Zebrafish*, 4(2):113–116, aug 2007. ISSN 1545-8547. doi: 10.1089/zeb.2007.0508.

[59] J.E. Turner. *Atoms, Radiation, and Radiation Protection: Third Edition*. Wiley-VCH, oct 2007. doi: 10.1002/9783527616978.

[60] S. Van Der Marck, D. Schaart, W. Van Der Zee, M. Tomsej, C. Van Vliet-Vroegindeweij, J. Jansen, M. Coghe, C. De Wagter, and B. Heijmen. Monte Carlo Treatment Planning An Introduction. Technical report, Nederlandse Commissie voor Stralingsdosimetrie, 2006. URL http://www.ncs-dos.org.

[61] M.C. Vozenin, P. De Fornel, K. Petersson, V. Favaudon, M. Jaccard, J. F. Germond, B. Petit, M. Burki, G. Ferrand, D. Patin, H. Bouchaab, M. Ozsahin, F. Bochud, C. Bailat, P. Devauchelle, and J. Bourhis. The Advantage of FLASH Radiotherapy Confirmed in Mini-pig and Cat-cancer Patients. *Clinical Cancer Research*, 25(1):35–42, jan 2019. ISSN 15573265. doi: 10.1158/1078-0432.CCR-17-3375.

[62] H. R. Withers. The Four R's of Radiotherapy. *Advances in Radiation Biology*, 5:241–271, jan 1975. ISSN 0065-3292. doi: 10.1016/B978-0-12-035405-4.50012-8. URL https://www.sciencedirect.com/science/article/pii/B9780120354054500128.

[63] C. Xu and L.I. Zon. 9 - The zebrafish as a model for human disease. In S.F. Perry, M. Ekker, A.P. Farrell, and C.J.B.T Brauner, editors, *Zebrafish*, volume 29, pages 345–365. Academic Press, 2010. ISBN 1546-5098. doi: S1546-5098(10)02909-2.

[64] T. Yabu, S. Todoriki, and M. Yamashita. Stress-induced apoptosis by heat shock, UV and γ-ray irradiation in zebrafish embryos detected by increased caspase activity and whole-mount TUNEL staining. *Fisheries Science*, 67(2):333–340, apr 2001. ISSN 09199268. doi: 10.1046/j.1444-2906.2001.00233.x.

[65] E.M. Zeman. The Biological Basis of Radiation Oncology. In *Clinical Radiation Oncology*, pages 2–40. Elsevier, 2016. doi: 10.1016/b978-0-323-24098-7.00001-0.

[66] O. Zlobinskaya, C. Siebenwirth, C. Greubel, V. Hable, R. Hertenberger, N. Humble, S. Reinhardt, D. Michalski, B. Roper, G. Multhoff, G. Dollinger, J.J. Wilkens, and T.E. Schmid. The effects of ultra-high dose rate proton irradiation on growth delay in the treatment of human tumor xenografts in nude mice. *Radiation research*, 181(2):177–183, feb 2014. ISSN 1938-5404 (Electronic). doi: 10.1667/RR13464.1.

A

Literature review

The introduction and background information has been edited out as the information is also provided in the rest of the thesis.

A.1. Method

For this review a literature search is executed in order to identify relevant studies. The search terms used are based on two main categories. The first category is radiation, specifically focused on high dose rate. The second category is biology, with a focus on organism and radiobiology. The search terms, represented in table A.1, are by category, every category has multiple search terms separated by OR and all the categories should be present in the search so the categories are added with an AND statement. This results in the following search term: (((((((photon OR proton OR electron OR irradiation OR "radiation therapy" OR "treatment dose" OR "irradiation dose" OR radiotherapy OR "photon beam" OR "proton beam" OR "electron beam"))))) AND (("dose-rate" OR "Ultra-high dose-rate" OR "FLASH"))) AND ((radiobiology OR "radiobiological respons" OR "radiobiological effectiveness" OR "dubble strand break" OR DBS OR "normal tissue toxicity" OR RBE OR apoptosis)) AND (dose-rate OR "Ultra-high dose-rate" OR "FLASH")).This search resulted in 648 papers for screening. Ten papers were supplied by the supervisors of this project, of which 4 are duplicates with respect to the database search. The titles and abstracts were considered eligible if they covered external high dose-rate radiation on biological tissue. The included articles were all in English, other languages were excluded. The literature search resulted in 14 papers used in the evaluation of the biological effect of high dose-rate radiation in this review, the search is visualized in a flow chart in figure A.1.

Table A.1: Search terms used in this literature search in Pubmed. The terms per category are separated by an "OR" statement, the catagories are seperated by an "AND" statement.

Radiation	photon proton electron irraiation "radiation therapy" "treatment dose" "Irradiation dose" radiotherapy "photon beam" "proton beam" "electron beam"	Biology	radiobiology "radiobiological respons" "radiobiological effectiveness" "dubble strand break" DSB "normal tissue toxicity" RBE apoptosis
Organisms	Zebrafish "Danio rerio" cells mice	Dose-rate	dose-rate "Ultra-high dose-rate" "FLASH"

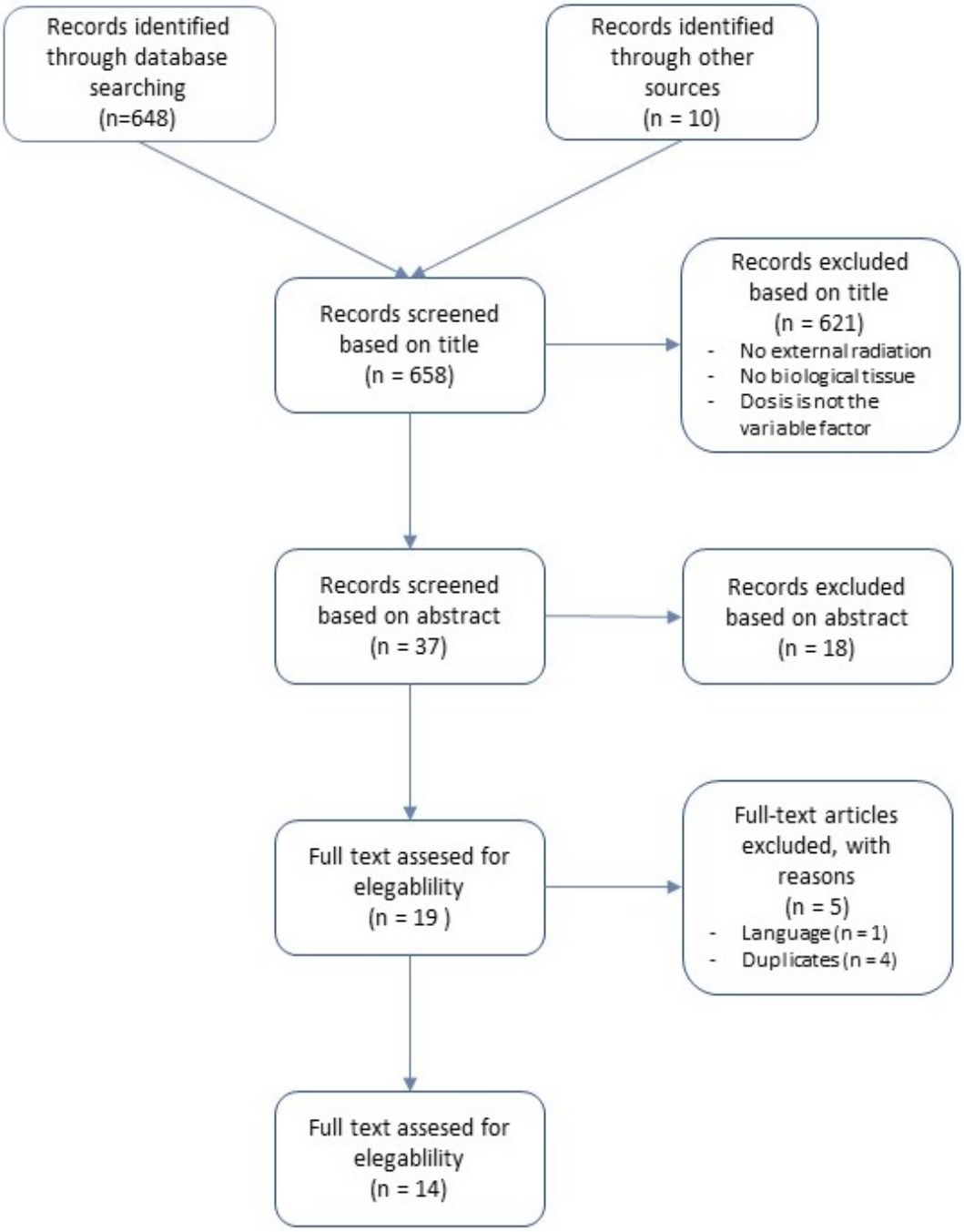

Figure A.1: Flow chart of the literature selection for this review

Table A.2: Key study characteristics and outcomes

Year	Author	Radiation type	Pulsed/ continuous	Energy	Dose rate	Total dose
2016	Laschinsky L	Electrons	Pulsed	1. 20 MeV 2. 3-20 MeV 3. 6 MeV	1. 0,4 Gy/min 3x 77 ns 2. techincal minimum irradiation time 3. mimics clinical LINAC	
2015	Beyreuther E	Electrons	Pulsed	20 MeV	10^10 Gy/min	4,8 and 2,4 Gy
2012	Laschinsky L	Electrons	Pulsed	6.5 MeV	peak dose-rate: 10^9 Gy/s	0,4-10,2 Gy
2013	Isaeva EV	Neutrons	Pulsed	14 MeV	0.8 mGy/min - 40 mGy/min	0.5-5Gy
2011	Lohse I	photon	Pulsed	10 MeV	20 cGy/min, 400 cGy/min & 2400 cGy/min	5 and 10 Gy
2010	Matsuura T	Protons			8 Gy/min & 325 Gy/min	1-8 Gy
2011	Auer	Protons	Pulsed	20 MeV	10^9 Gy/s	3 Gy
2015	Favaudon V	Electrons	Pulsed		40 Gy/s	1. 17 Gy 2. 16 to 30 Gy FLASH dose escalation
2018	Hao J	Photon		6 Mev	21.2 Gy/min	2,4,6 Gy
2014	Zlobinskaya O	Protons	Pulsed & contiuous	23 MeV		20 Gy
2016	Schuller E	Electrons	Pulsed	20 MeV & 9 MeV	max of 900 Gy/s	
2015	Gagnaire B	Photons	Continuous		570 mGy/h and 0,8 mGy/h	
2017	Hurem S	Photons	Continuous		0.4 mGy/h, 38 mGy/h	17.5 - 3496 mGy
2008	Jang	Protons	Continuous	35 MeV		1,2 and 5 Gy

Continuation of key study characteristics and outcomes

Author	Pulsed/ continuous	C. energy	C. dose rate	C. total dose	Evaluation method	Organism/cells	Findings
Laschinsky L					DSB, SF	Cells	No considerable differences in RBE
Beyreuther E	Continuous			4,8 and 2,4 Gy	DSB, SF	Cells	No considerable differences in RBE
Laschinsky L	Continuous	6 MeV	3 Gy/min		SF, DSB	Cells	No considerable differences in RBE
Isaeva EV	Continuous			0.5-5Gy	SF, DSB	Cells	No considerable differences in RBE
Lohse I					SF	Cells	High dose-rate has a high RBE
Matsuura T					SF and RBE	Cells	No considerable differences in RBE
Auer	Continuous			3 Gy	SF and RBE	Cells	No considerable differences in RBE
Favaudon V	Continuous	4.5 MeV	0.03 Gy/s	15 and 17 Gy	Macroscopic lesions, DSB and apoptosis, tumor control	Mice	Pulsed irradiation has preferential RBE compared to continuous
Hao J		6 Mev	4.2 Gy/min	2,4,6 Gy	Macroscopic, DSB, cell cycle distribution	Mice	No considerable differences in RBE
Zlobinskaya O	Continuous	6 MV		20 Gy	Growth delay and RBE	Mice	No considerable differences in RBE
Schuller E					None	Purely physical	
Gagnaire B			No dose		1. Macroscopic 2. DSB, apoptosis 3. immunotoxic and neurotoxic biomarkers 4. gene expression 5. histopathological	Zebrafish	Low dose radiation has a RBE on zebrafish
Hurem S					RNA expression, macroscopic	Zebrafish	High mortality with high dose-rate; More deformaties with low dose-rate
Jang					Bloodvessel growth	Zebrafish	Higher dose, higher RBE

A.2. Evaluation of the literature

This review contains a study of articles on four different radiation types, protons, electrons, photons and neutrons and three different biological media, cells, mice and zebrafish. It also contains information about the anatomy and physiology of zebrafish and some information about Monte Carlo simulations.

A.2.1. Comparison of radiotherapeutical methods

All the selected articles are compared based on radiation type, total dose, dose-rate, fractionation, evaluation method, time between the radiation and the evaluation. A summary of the articles can be found in tabel 4.1.

Six of the studies incorporated in this review have been conducted using electrons. Three of these have been done using in vitro cells. Laschinsky uses fibroblast in a study from 2016 [40], the same group uses carcinoma cells in a 2015 study [6] and compares tumor and normal tissue cells in a study in 2012 [39]. These three studies all have a pulsed dose with a pulse dose rate of about 10^{10} Gy/min. In these studies all the cells are evaluated on double strand breaks, surviving fraction and cell colony formation. The double strand breaks are evaluated using $\gamma H2AX/53BPI$ foci analysis, which is an immunohistochemical technique. Colonies were categorized as colonies when they contained more than 50 cells. The surviving fraction is calculated using $SF(D) = e^{-\alpha D-\beta D^2}$ where α and β are fitted using the experimental data. All three articles found no considerable differences in radiobiological effectiveness between the high dose-rate and the and the conventional irradiation schemes. However the Laschinsky et al. [39] article found one cell line where the DSB effectiveness was reduced with high dose-rate irradiation. The articles did not specify a fractionation scheme suggesting that all the dose was given in one fraction. The DSB assays were done directly after irradiation, this means that the regenerative capabilities of the cells were not investigated.

Other research on this topic that has been conducted on cells was done using photon irradiation of normal tissue cells [41]. In this article three different dose-rates have been investigated on normal tissue human submandibular gland (HSG) cells. The surviving fraction regarding dose-rates of 20 cGy/min, 400 cGy/min and 2400 cGy/min was determined using colonic cell survival. In order to evaluate the radiation damage a colony assay was executed and the linear quadratic model was fitted in order to estimate α and β. The colonic assay was executed 10-14 days after irradiation. The radiation dose was 5 and 10 Gy, again, no information about fractionation was provided. Therefor we have to assume all the radiation was given in one fraction. This study found that colonic cell survival is reduced when a higher dose per pulse is used, while keeping the mean dose and the delivery time constant.

Cell irradiation is also investigated using proton radiation of 8 Gy/min and 325 Gy/min with a total dose between 1 and 8 Gy [42]. The cells used in this experiment are normal tissue HSG cells, which is the same cell type used in Lohse et al. [41], however this paper irradiated the cells using protons instead of photons. The difference in cell survival was investigated by estimating the α and β based on the experimental data. The paper does not clearly state how much time there is between the irradiation and the survival curve, however the researchers suggests that there is thirteen days between irradiation and the evaluation. This paper found no difference in cell survival curves between the dose-rates, it however did find a better radiobiological effectiveness in the Bragg peak than in the plateau, before the Bragg peak. This result is consistent with what is known about the dose deposition curves for protons. Another paper that investigated the radiobiological effect of protons is [4], however the investigated cells are Hela tumor cells. The dose-rates used in this research is 109 Gy/s and a total dose of 3 Gy. This paper evaluated the cells not only on surviving fraction or double stranded breaks but also on cell cycle distribution. This paper compared pulsed high dose-rate 109 Gy/s to continuous radiation which had a dose-rate of 30 Gy/s. The radiobiological effects are evaluated based on cell cycle arrest and apoptosis, cell cycle distribution and colonic survival. The incubation times were 10, 24 and 48 hours and the differences in repair time were taken in to account in their findings. It found no significant difference in radiobiological effectiveness between the high dose-rate and conventional radiation.

Three articles are included in this literature review that analyzed mice irradiation one, on electron irradiation, one on photon irradiation and one on proton irradiation. The article regarding electron radiation [20] has xenografted human tumors on mice. A caspase-3 and a TUNEL assay is conducted to assess the biological effectiveness. The biological effectiveness was monitored until 36 weeks after irradiation. This study found that delivery time is a determinant of normal tissue toxicity and high dose-rate irradiation enhances differential responses between normal and tumor tissues. Another article [29] considered photon irradiation on xenografted mice. The tumors were irradiated with varying dose rates and varying total doses. This study found no significant differences in cell viability between the dose rates. The article studying proton radiation [66] compares pulsed protons with conventional radiotherapy, the mice receive a total dose of 20 Gy. It asses

the radiobiological effectiveness based on tumor growth delay and the RBE. The tumor growth was monitored for 120 days after proton irradiation. No statistical difference was found in radiobiology between the pulsed and the continuous irradiation.

There are two articles included that investigated the effects of radiation on zebrafish [24, 35]. They both used an acridine orange staining [58]. Acridine orange is a large scale analysis of apoptosis based on a optical analysis, it binds to the chromatin of dying cells. Devaux et al. [15] developed a method to detect DNA breaks using a comet assay that is applied by Gagnaire et al. [24] to get a good estimate on the DNA damage. Gagnaire et al. [24] also measures immunotoxicity and neurotoxicity by measuring phenoloxidase (PO) like activity using L-dopa, other biotoxicity measures were on ethoxyresorufin-O-deethylase (EROD) and rective oxygen spieces (ROS) activity.

In an article published by Gagnaire et al. in 2013 [23] the methods to measure the immunotoxicity is described. The methods for measuring activity in adult fish was different then from the larvae. The article describes methods for adult fish and larvae, however for the purposes of this literature review only the methods using larvae are described considering the limitations for this research to larvae. The PO activity was measured using a 96 well plate containing one living larva and adding CAC and L-dopa to each well. The larvae were incubated and absorbance was measured at 490 nm every hour for a total of 24 hours. The assessment of the larvae was based on movement in order to check if they are alive after the 24 hour period.

The article uses photon irradiation with two dose rates of continuous radiation: a dose-rate below the IAEA [32] limit of 0.10 mGy/day for freshwater organisms and one dose-rate above the limit. The two dose-rates are 0.08 and 570 mGy/day. The zebrafish are irradiated for four days prior to the assessment of the biological effects. The article on proton radiation irradiates the tail of zebrafish with a total dose of 1,2 and 5 Gy, the rest of the fish are shielded. The blood vessel formation and the macroscopic appearance of the tail is investigated. Both articles investigate oxidative stress, while the previously mentioned articles [4, 6, 19, 20, 29, 39, 41, 42, 66], on cell irradiation and tumor irradiation in mice did not take oxidative stress in to account. Gagnaire et al. also took gene expression in to account using qPCR.Hurem et al [31] investigated the gene expression as a result of gamma radiation. Besides the microscopic properties of radiation damage the macroscopic properties are be taken in to account as well, like motility, hatching and physical appearance.

A.2.2. Evaluation of biological essay techniques

A variety of biological assays is used for different evaluation methods. These assays help asses the radiobiological effect on tissue. An overview of different possible assay techniques is discussed.

A comet assay is used to detect general levels of DNA damage [50]. It is an electrophoresis technique in which the DNA is unwinded, usually through a high pH, and then embedded in agarose and electrophoresis is applied [12]. This procedure result is a “halo” that can be used to quantify the amount of DNA damage. The visualization procedure can be executed using different types of fluorescent dyes. Gagnaire et al. [24] used trypan blue, according to Collins et al. [12] the most commonly used is Etherium bromide (EB). Another common one is DAPI that binds to the DNA, where EB binds most efficient to double stranded breaks. The comets are often evaluated based on the tail length, relative fluorescence intensity of head and tail, and tail moment [12]. Besides quantification it is also possible to visually score the comets, where Collins et al. [12] showed that there is a close relationship between the visual scoring and the evaluation based on image analysis techniques and visual scoring done by volunteers [11]. This method of DNA damage assessment can be useful in a number of ways and can be applied in ecological and human studies. It can also monitor DNA repair.

The TUNEL assay was originally developed by Gorczyca et al. [26] uses an enzyme, DNA polymerase or exogenous terminal transferase to label 3’ -OH termini with biotinylated dUTP. TUNEL stands for Terminal deoxynucleotidyl transferase dUTP nick end labeling. The method uses a fluorochrome to tag the double stranded DNA breaks. In combination with a caspase-3 assay, the TUNEL assay can be used to identify apoptotic cells [16]. Caspase-3 is frequently present in many cell types when apoptosis is induced [49]. Caspase-3 detection can be done by antibody or substrate based methods.

The EROD activity is measured using an 7-ethoxyresorufi (ER) solution, according to a protocol developed by Noury et al. [47]. The ER solution is added to 2 mL synthetic water in a 24-well microplate with a larvae in each well. The final concentration is 1.5 µM. 100 µL of this solution is immediately transferred to a 96 well plate including the larvae to measure the excreted resorufin (RR). The resorufin is detected at 587 nm with a 545 nm excitation wavelength, this minimizes the ER fluorescence. The amount of RR is calibrated by a standard curve of RR.

The ROS production is measured using the oxidation of a non-fluorescent dye to a fluorescent prod-

uct, according to a protocol by Hermann et al. [30]. The substrate used is 5- (and 6-)chloromethyl-2',7'-dihydrodichlorofluorescein diacetate (CM-H2DCFA) and is oxidized to dichlorofluorescein (DCF). According to the protocol are the embryos incubated in a 2.5 µg/ml neutral red at 28 °C for 24 hours. After the incubation time CM-H2DCFA and PMA are added to final concentrations of 500 and 200 ng/ml, respectively, and incubated for 60 minutes. The yolks are dissected and mounted on slides, the CM-H2DCFA is excited at 485 nm fluorescens and the emission is observed at 530 nm. Using a microscope the fluorescence is observed and measured.

A.2.3. Overview of Monte Carlo dose calculations

Monte Carlo codes offer a great way to model the dose deposition inside tissue. The model has the possibility to account for all the possible interactions with materials with different densities. Using this method the radiation inside the zebrafish can be accurately calculated.

There are simpler faster methods available in which a pencil beam kernel is calculated using Monte Carlo simulations and that kernel is then convoluted with the total energy release per unit mass (TERMA) of the medium. However complete Monte Carlo dose calculations are more precise although computationally more expensive. They model the dose deposition in the medium by calculating the radiation emitted by the source. Both the energy and the angle of the radiation is determined using the energy spectrum and the angular information. This radiation results both in a dose in the target, but can also result in secondary particles that contribute to the dose in the target. The radiation emitted directly from the source is the "primary energy fluence". [48]

In dosimetry calculations Monte Carlo codes are the gold standard, since they do not rely on any assumptions but calculate each individual ionizing particle moving through a medium. For modeling of a beam each particle is individually modeled. Particles are initialized, with certain energy and angle, their path is determined and the interaction are sampled. Monte Carlo simulations can be done using any type of particle, so it can be done for photons, electrons and protons, for instance. [48]

For the first step of the Monte Carlo calculations the particles are mimicked using known energy and angular distribution. The energy and the angle of the individual source particles model the primary energy fluence. Once the primary energy fluence is modeled, the interactions of this radiation with the surroundings can be calculated. Different radiation types have different physical characteristics and therefor different dose deposition. Using known probabilities distributions of the physical processes of the particles the interaction can be calculated. In order to calculate the interaction both the path length of the primary particle and the type of interaction is sampled. The path length and the type of interactions determine the dose deposition in the surroundings. The path length is calculated using the attenuation coefficient, which is depended on the type of the material and the energy of the radiation. All these parameters are sampled form known probability distributions using a random number generator. The sampling from a known distribution is the basis of the Monte Carlo calculations. [60]

There a different Monte Carlo codes available the main difference between these codes is the assumptions that are made with respect to the handling of electrons. Electrons are computationally more expensive because there have a lot more interactions than other radiation types. Monte Carlo codes simplify the electron interactions in order to reduce the computational power, resulting in different Monte Carlo codes. The most critical issue for Monte Carlo codes is the handling of boundary crossings. Monte Carlo codes are often assessed on how they handle boundary crossings. At an interface different densities occur resulting in backscatter and boundary crossing. Both of these principles should be handled correctly.[51]

The code used in this research is the MCNP code, which was originally developed for neutron-photon transport, used in reactor calculations. It has a powerful geometry package and can be adapted to medical physics purposes [51].

A.3. Discusison

This literature review investigated the published literature of the last ten years on the effects of ionizing radiation on cells, zebrafish and mice. The motivation of this review is to investigate the biological effects of high dose-rates ionizing radiation on zebrafish.

Zebrafish grow during a five day period in which they are mostly transparent, making them ideal organisms for developmental studies. As they are used in many environmental and toxicology studies. The developmental morphology and physiology of healthy and unhealthy zebrafish are mostly know, as they are a model organism with sequenced DNA.

All the articles selected for this literature review concern the biological effects of high dose-rate radiotherapy. Both the methodology and the organisms used in the experiments are diverse. The articles include cells, zebrafish and mice. These three organisms are relevant model organisms in this research niche. The dose-rates used in the articles range between less than a milli-Gray per hour and 10^{10} Gray per hour. In the literature there seems no agreement on the definition on when the dose-rate of irradiation is high enough to qualify as high dose-rate irradiation. The types of radiation are also diverse: photons, protons, neutrons and electrons. As a result of the diversity in radiation type and dose-rate the articles hard to compare. However there are more differences in the methodology resulting in a difficult comparison. The types of evaluation are diverse, some because of the different organisms, some because of different choices in the evaluation methodology by the auteurs. Another key difference that is how long the evaluation of the tissue was after the irradiation of the sample. Since biological tissue has regenerative capabilities the amount of DNA damage and other markers for cell damage can have been repaired. Depending on the goals of the research either acute or late effects of radiation can be relevant. This research aims to supply supporting information for high dose-rate irradiation the regenerative capabilities of tissues should be taken in to account.

Another known factor to radiation damage is the oxygen tension inside the cell. However none of the articles took it in to account. In vivo the oxygen in blood is regulated by physiological principles, but in vitro the oxygen tension could need some regulation, depending on the way the sample is prepared. Only one article took the cell cycle evaluation into account even though it is one of the main reasons a fractionation is applied.

All the articles took a single fraction in to account. However it is crucial to investigate the difference in the biological effect of different amounts of fractionation before high dose-rates combined with low fractionation can be applied in a clinical setting.

When assessing radiation damage, one of the first markers are DNA breaks. Especially double stranded DNA breaks are important perpetrators of apoptosis. There are several methods that can be employed to detect DNA breaks. Three different detection methods have been used to detect in three different articles. The comet assay, and the TUNEL assay and $\gamma H2AX/53BPI$ foci immunostaining technique. The TUNEL assay in combination with caspase-3 can also be used as a biomarker for apoptosis, as well as acridine orange. So there are a lot of different DNA break detection techniques. Some can be specified for single or double stranded breaks based on the substrate chosen in the assay. All of these techniques, especially the ones that are specific for double standed breaks, are a biomarker for apoptosis, however it is not a definite biomarker since double stranded breaks can be repared and apoptosis is not inevitable.

An inderect measurement of apoptosis are colony assays. In a colony assay the number of surviving cells can be determined, instead of the numer of dead cells. The downside of colony assays is that they can only be done in vitro. For in vivo DNA damage assement one of biological assays discussed is a suitable evaluation method. The advantage of colony assay technique is that the linear quadratic model can be applied to the data, providing more information about dose dependencies and difference in conditions that are relevant to radiation damage. The colony assay is used in all the articles that concern cell experiments. Proteins have been labeled to visualize certain structures [24, 35] depending on what features the researchers are interested in.

Monte Carlo dosimetry calculations are the gold standard in dosimetric calculations. They have the ability to determine the dose deposition inside the target by sampling each individual particle. A lot of resources, like MCNP, are available to be used in radiotherapeutic research in the medical physics field.

A.4. Conclusion

As only a limited amount of research has been done regarding ionizing radiation in zebrafish embryos, additional model organisms are researched get a more complete overview of the methodology of radiobiological research. For this literature review mice and cells are included to extend the scope of this review. This review concludes that it is possible to investigate the effects of ionizing radiation in zebrafish. This can be done both on a macroscopic scale, motility, hatching, survival and on a microscopic scale, double strand breaks, protein expression.

Form the literature is concluded that it is possible to conduct radiotherapeutical research in Zebrafish. The precise dose-rate effects of ionizing radiation is not clear from this review as the results vary. Eight of the fourteen articles found no considerable differences in RBE between high dose-rate and conventional radiotherapy. Three of the fourteen articles found that high dose-rate radiotherapy has a higher RBE with respect to conventional radiotherapy. The last three articles did not directly compare high dose-rate with conventional radiotherapy.

More research is needed to deepen the current level of understanding on the biological effects of high dose-rate ionizing radiation. This research will provide more data and help deepen the understanding of these concepts.

B

MCNP code

```
DishET
c cell cards for cylinder problem
1  3 -0.00125   -1 2 10 11 12 13 ... 31 32 33      imp:p,e =1 $outer cobalt cylinder
2  3 -0.00125   -2 6                               imp:p,e =1 $ inner air cylinder
3  0             50:-51:-52:53:54:-55              imp:p,e =0 $ void outside
4  4 -11.34     -40 41 42 -43 -44 45 1            imp:p,e =1 $ lead container
5  3 -0.00125   -50 51 52 -53 -54 55 (40:-41:-42:43:44:-45) imp:p,e =1 $ lead
6  1 -1         -6                                imp:p,e =1 $ water inside dish
7  6 -1          6 -2                             imp:p,e =1 $ plastic dish  rims
10 2 -8.9       -10                               imp:p,e =1
11 2 -8.9       -11                               imp:p,e =1
12 2 -8.9       -12                               imp:p,e =1
13 2 -8.9       -13                               imp:p,e =1
14 2 -8.9       -14                               imp:p,e =1
15 2 -8.9       -15                               imp:p,e =1
16 2 -8.9       -16                               imp:p,e =1
17 2 -8.9       -17                               imp:p,e =1
18 2 -8.9       -18                               imp:p,e =1
19 2 -8.9       -19                               imp:p,e =1
20 2 -8.9       -20                               imp:p,e =1
21 2 -8.9       -21                               imp:p,e =1
22 2 -8.9       -22                               imp:p,e =1
23 2 -8.9       -23                               imp:p,e =1
24 2 -8.9       -24                               imp:p,e =1
25 2 -8.9       -25                               imp:p,e =1
26 2 -8.9       -26                               imp:p,e =1
27 2 -8.9       -27                               imp:p,e =1
28 2 -8.9       -28                               imp:p,e =1
29 2 -8.9       -29                               imp:p,e =1
30 2 -8.9       -30                               imp:p,e =1
31 2 -8.9       -31                               imp:p,e =1
32 2 -8.9       -32                               imp:p,e =1
33 2 -8.9       -33                               imp:p,e =1

c surface cards for cylinder problem
1  RCC  0    0    0   0 0 55.4 7.2
2  RCC  0    0    0   0 0 55.4 4.45
6  RCC  0    0    5.1 0 0 0.8  2.3
7  RCC  0    0    5   0 0 1    2.5
```

```
40 PY   30.48
41 PY  -30.48
42 PX  -30.48
43 PX   30.48
44 PZ   55.40
45 PZ  -90.42
50 PY   40.64
51 PY  -40.64
52 PX  -40.64
53 PX   40.64
54 PZ   55.40
55 PZ  -98.91
10 RCC  6.1  0    0 0 0 12.9 0.4
11 RCC  5.9  1.6  0 0 0 12.9 0.4
12 RCC  5.3  3.1  0 0 0 12.9 0.4
13 RCC  4.3  4.3  0 0 0 12.9 0.4
14 RCC  3.1  5.3  0 0 0 12.9 0.4
15 RCC  1.6  5.9  0 0 0 12.9 0.4
16 RCC  0    6.1  0 0 0 12.9 0.4
17 RCC -1.8  5.9  0 0 0 12.9 0.4
18 RCC -3.1  5.3  0 0 0 12.9 0.4
19 RCC -4.3  4.3  0 0 0 12.9 0.4
20 RCC -5.3  3.1  0 0 0 12.9 0.4
21 RCC -5.9  1.6  0 0 0 12.9 0.4
22 RCC -6.1  0    0 0 0 12.9 0.4
23 RCC -5.9 -1.6  0 0 0 12.9 0.4
24 RCC -5.3 -3.1  0 0 0 12.9 0.4
25 RCC -4.3 -4.3  0 0 0 12.9 0.4
26 RCC -3.1 -5.3  0 0 0 12.9 0.4
27 RCC -1.6 -5.9  0 0 0 12.9 0.4
28 RCC  0   -6.1  0 0 0 12.9 0.4
29 RCC  1.6 -5.9  0 0 0 12.9 0.4
30 RCC  3.1 -5.3  0 0 0 12.9 0.4
31 RCC  4.3 -4.3  0 0 0 12.9 0.4
32 RCC  5.3 -3.1  0 0 0 12.9 0.4
33 RCC  5.9 -1.6  0 0 0 12.9 0.4

c Materials used in cell definition
M1   1000   2    8000 1                    $H20
M2   27060  1                              $Co60
M3   14000  7808 16000   2096 18000 93     $Air
M4   82000  1                              $Lead
M5   6000   24   1000    236   8000  118   $Agar(C12H20O10)2% With Water
M6   6000   8    1000    8                 $Plastic
c ------------------------------------------------
c Physics cards
c Particles: Photons, Electrons
MODE P E
c Cut off - needed for electron FMESH
PHYS:E  500. 6j 0
cut:e j 1e-3
c Stopping criterium
NPS 10000000
c ------------------------------------------------
c Source defenition
c Explicitly defined using SI and SP cards of SDEF
```

```
SDEF ERG D1 cell=D4 par=2 rad D2 axs= 0 0 1 ext D3 pos=Fcel=D5
SI1   l   1.332 1.173                    $ sample energy
SP1       1     1
SI2   h   0     0.4                      $ sample rad uniformly
SP2      -21    1
si3   h   0     12.9                     $ sample height uniformly
sp3      -21    0
SI4   l   10 11 12 ... 30 31 32 33       $ sample cell
SP4       625 684 767 ...  637 625 661
DS5   S   10 11 12 ... 30 31 32 33
SI10  l   6.10 0.00 0
SP10      1
SI11  l   5.89 1.58 0
SP11      1
SI12  l   5.28 3.05 0
SP12      1
SI13  l   4.31 4.31 0
SP13      1
SI14  l   3.05 5.28 0
SP14      1
SI15  l   1.58 5.89 0
SP15      1
SI16  l   0.00 6.10 0
SP16      1
SI17  l  -1.58 5.89 0
SP17      1
SI18  l  -3.05 5.28 0
SP18      1
SI19  l  -4.31 4.31 0
SP19      1
SI20  l  -5.28 3.05 0
SP20      1
SI21  l  -5.89 1.58 0
SP21      1
SI22  l  -6.10 0.00 0
SP22      1
SI23  l  -5.89 -1.58 0
SP23      1
SI24  l  -5.28 -3.05 0
SP24      1
SI25  l  -4.31 -4.31 0
SP25      1
SI26  l  -3.05 -5.28 0
SP26      1
SI27  l  -1.58 -5.89 0
SP27      1
SI28  l   0.00 -6.10 0
SP28      1
SI29  l   1.58 -5.89 0
SP29      1
SI30  l   3.05 -5.28 0
SP30      1
SI31  l   4.31 -4.31 0
SP31      1
SI32  l   5.28 -3.05 0
SP32      1
```

```
SI33  l   5.89 -1.58 0
SP33      1                                  $ position of every cell in order
c -------------------------------------------------------
c Tally specifications
F16:P  6                              $ energy deposition of photons Mev/gram
F26:E  6                                    $ energy deposition of electrons Mev/gram
+F106  6                                    $ energy deposition of all particles
FMESH14:P  GEOM=xyz       ORiGIN= -6.1 -6.1 -1
         imesh 6.1 iints 123
         jmesh 6.1 jints 123
         kmesh 14  kints 151
         OUT=IJ
FM14 -1 0 -5 -6
FMESH24:P GEOM=xyz       ORiGIN= -3 -3 4.5
         imesh 3 iints 121
         jmesh 3 jints 121
         kmesh 6.5 kints 41
         OUT=IJ
FM24 -1 0 -5 -6
c Diedrick's FMESH for electrons
FMESH154:e ORIGIN=-3 -3 4.5
           imesh 3 iints 61
           jmesh 3 jints 61
           kmesh 6.5 kints 21
           OUT=IJ FACTOR=1
FMESH164:e ORIGIN=-6.1 -6.1 -1
           imesh 6.1 iints 61
           jmesh 6.1 jints 61
           kmesh 14  kints 76
           OUT=IJ FACTOR=1
DE154 LOG
     1.0790E-03
     1.1766E-03
     1.2831E-03
     ...
DF154 LOG
     1.129E+02
     1.068E+02
     1.009E+02
     ...
DE164 LOG
     1.0790E-03
     1.1766E-03
     1.2831E-03
     ...
DF164 LOG
     1.129E+02
     1.068E+02
     1.009E+02
```

C

Immunostaining protocols

General procedure

1. Evening before: Set-up crossing
2. 0- 5 hpf: Collect embryos
3. 24 hpf: Treatement with radiation and Thapsigargon
4. 30 hpf: Fixation of embryos
5. 3 dpf: Fixation of embryos
6. Staining of embryos according to protocols below
7. Mounting in 100% glycerol of 2% agarose
8. Imaging

Fixation procedure 30 hpf embryos

Time	**Operation**
3 minutes	Incubate in 10 mg/ml pronase at 28 °C swirl around to dechorionate
10 minutes	Wash 4 times in egg water
1 hour	Euthenize embryos
2 hours	Fixate in 4% PFA at room temperature
15 minutes	Wash in PBS 3 x 5 minutes
3 x 5 minutes	Dehydrate through graded methanol series 25%, 50%, 75%
	Store in 100% methanol

Fixation of 3 dpf embryos

Time	Operation
1 hour	Euthenize embryos
30 minutes	Incubate in 2 mg/ml pronase at 28 °C
10 minutes	Wash 4 times in egg water
2 hours	Fixate in 4% PFA at room temperature
3 x 5 minutes	Wash in PBS
3 x 5 minutes	Dehydrate through graded methanol series 25%, 50%, 75% 5 minutes in each solution
	Store in 100% methanol

Rehydration and permabilization

Time	Operation
20 minutes	Rehydrate through graded methanol series 75%, 50%, 25% 5 minutes in each solution
30 hpf: 20 minutes 3dpf: 60 minutes	permabilize with 0.2% collagenase in PBS with 0.5 mM of calciumcholoride on a rocking platform
3 x 5 minutes	Wash in PBSTw

Caspase-3

Time	Operation
2 hours	Incubate with blocking agent PBSTw + 10% goat serum
Overnight	Incubate with primairy anti-body on a rocking table 1 mL PBSTw 10 µL goat serum 1 µL primairy anti-body
4 x 15 minutes	Wash with PBSTw
4 hours	Incubate with secondairy anti-body on a rocking table 1 mL PBSTw 10 µL goat serum 2.5 µL secondairy anti-body
4 x 20 minutes	Wash with PBSTw
3 x 5 minutes	Wash with PBS
	Store in PBS until imaging

TUNEL

Time	Operation
30 hpf: 60 minutes 3 dpf: 1 hour	Incubate in TUNEL solution (per eppendorf) 10 µL reaction buffer 0.75 µL TdT enzyme 8 µL FITC 32.23 µL MilliQ Control without TdT
3 x 5 minutes	Wash with PBSTw
	Store in PBS until imaging

DAPI staining

Time	Operation
30 hpf: 20 minutes 3 dpf: 60 minutes	Incubate in DAPI 1 µL DAPI 5 mL PBS
3 x 5 minutes	Wash with PBSTw
	Store in PBS until imaging

D

Controls to different times of radiation experiment

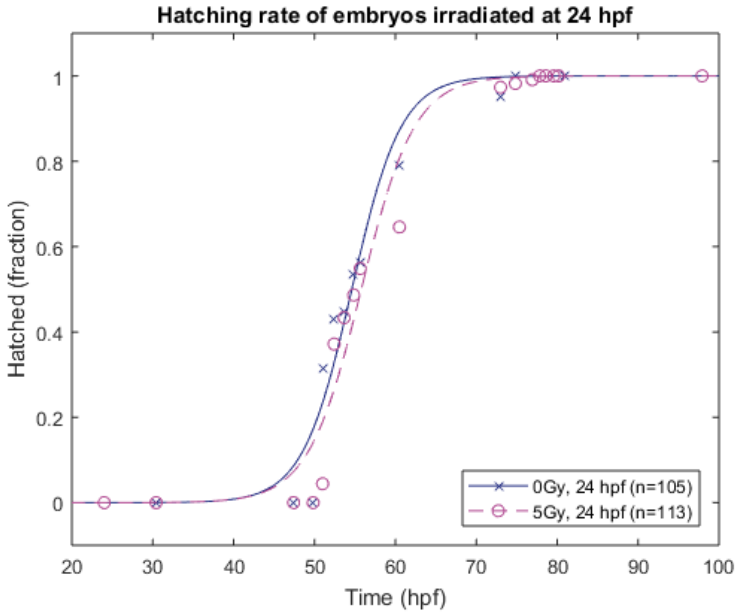

Figure D.1: Hatching rate of embryos that received 5 Gy with a dose-rate of 0.015 Gy/s and the control at 24 hpf

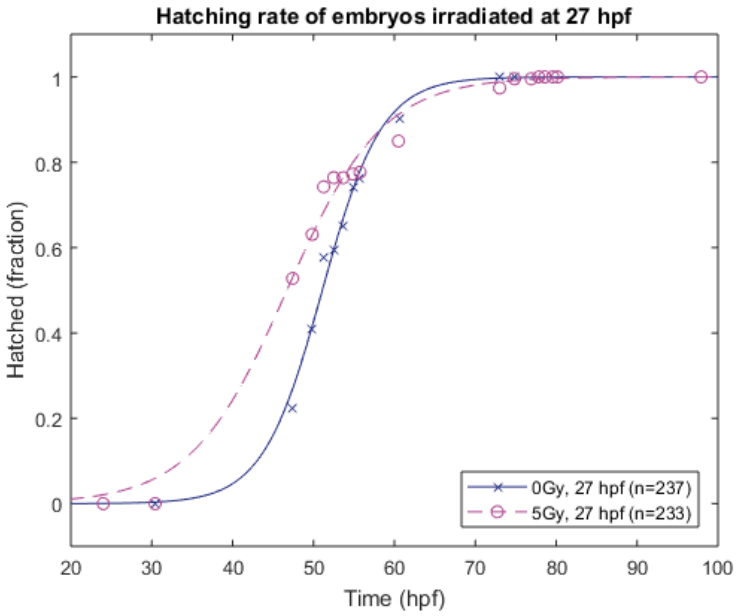

Figure D.2: Hatching rate of embryos that received 5 Gy with a dose-rate of 0.015 Gy/s and the control at 27 hpf

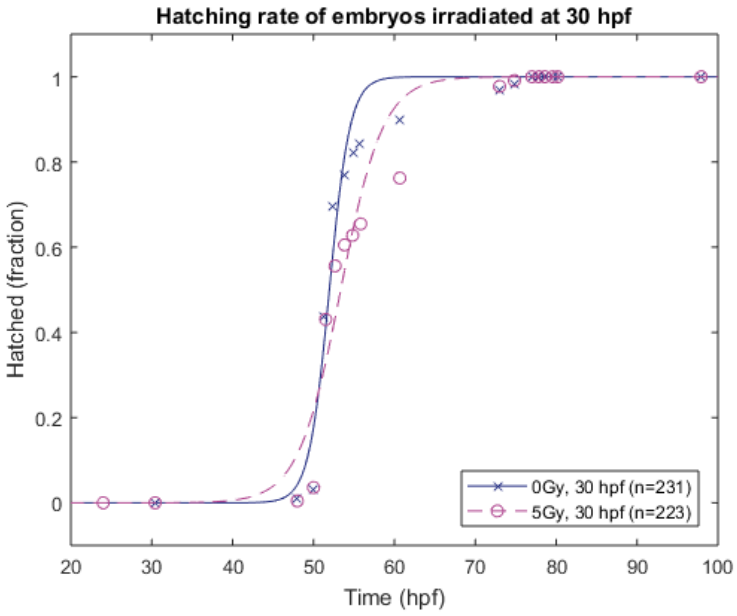

Figure D.3: Hatching rate of embryos that received 5 Gy with a dose-rate of 0.015 Gy/s and the control at 30 hpf

E

ImageJ scripts

This script treshold images at a set treshold and then preforms a bit wise AND comparison between the DAPI and the staining. The entire zstacks are measured and saved. The results of the measurements are shown in the result section of the thesis.

```
run("Close All");

dir1 = getDirectory("Choose Directory with zstacks ")
dir2 = getDirectory("Choose Directory to save MAX projections: ");
//dir3 = getDirectory("Choose Directory to save measurement results: ");
list = getFileList(dir1);
setBatchMode(true);

for (i=1; i<30; i++)
{
        run("Close All");

        filename = dir1+list[i];
        open(filename);

        filename = dir1+list[i];
        open(filename);
        selectImage(4);
        name=getTitle();
        rename(name+"-2");

        selectImage(5);
        name=getTitle();
        rename(name+"-2");

        selectImage(6);
        name=getTitle();
        rename(name+"-2");


// DAPI

        selectImage(1);
        setAutoThreshold("Default dark no-reset");
        //run("Threshold...");
        setThreshold(220, 65535);
```

```
        run("Convert to Mask", "method=Default background=Dark calculate black");

        selectImage(1);
        run("Divide...", "value=255.000 stack");

        run("32-bit");
        setThreshold(1.0000, 1000000000000000000000000000000.0000);
        run("NaN Background", "stack");;

        mask = getTitle();

        selectImage(4);
        original = getTitle();
        imageCalculator("Multiply create stack", mask, original);
        selectImage(7);
        run("Measure Stack...");
//        saveAs("Results", dir3+list[i]+"_DAPI.csv");
        run("Clear Results");
        run("Z Project...", "projection=[Max Intensity]");


// Staining

        selectImage(2);
        setAutoThreshold("Default dark no-reset");
        //run("Threshold...");
        setThreshold(220, 65535);
        run("Convert to Mask", "method=Default background=Dark calculate black");

        selectImage(2);
        run("Divide...", "value=255.000 stack");

        run("32-bit");
        setThreshold(1.0000, 1000000000000000000000000000000.0000);
        run("NaN Background", "stack");

        mask = getTitle();

        selectImage(5);
        original = getTitle();
        imageCalculator("Multiply create stack", mask,original);
        selectImage(9);
        run("Measure Stack...");
//        saveAs("Results", dir3+list[i]+"_Stain.csv");
        run("Clear Results");
        run("Z Project...", "projection=[Max Intensity]");
//        run("Measure");


//         Combination of DAPI and staining
        selectImage(7);
        dapi = getTitle();

        selectImage(9);
        staining = getTitle();
```

```
        imageCalculator("AND create 32-bit stack", dapi, staining);
        selectImage(11);
        run("Measure Stack...");
//        saveAs("Results", dir3+list[i]+"_Comb.csv");
        run("Clear Results");
        selectImage(11);
        run("Red Hot");
        run("Z Project...", "projection=[Max Intensity]");
        run("8-bit");
        run("Red Hot");

        saveAs("Tiff", dir2+"Comb_"+list[i]+".png");

}
```